



**DE-EE-0006746**

**Project Title:** Geothermal Thermoelectric Generation (G-TEG) with Integrated Temperature Driven Membrane Distillation and Novel Manganese Oxide for Lithium Extraction

**Project Period:** October 1, 2014 to June 30, 2016

**Budget Period:** October 1, 2014 to June 30, 2016

**Reporting Period:** October 1, 2014 to June 30, 2016

**Submission Date:** September 30, 2016, Resubmitted April 28, 2017

**Recipient:** Southern Research; DUNS Number: 00-690-0526; 2000 Ninth Avenue South, Birmingham, Alabama 35205-2708

**Award Number:** DE-EE0006746

**Project Team:** Southern Research, Novus Energy Technologies, Carus Corporation, and Applied Membrane Technology, Inc.

**Principal Investigators:** Mr. Jay E. Renew, P.E.  
jrenew@southernresearch.org  
(Silica Removal, Nanofiltration, Membrane Distillation, and Mn-Oxide Sorbent)

Mr. Tim Hansen, P.E.  
thansen@southernresearch.org  
(Thermoelectric Power Generation and Technical and Economic Analysis)

**Business Contacts:** Ms. Nancy Thompson., Contract Administrator,  
nthompson@southernresearch.org

**DOE Contracting Officer:** Mr. Andrew Rittgers

**DOE Project Officer:** Mr. Tim Reinhardt

**Project Monitor:** Ms. Sara Emmons

## 1.0 EXECUTIVE SUMMARY

Southern Research Institute (Southern) teamed with partners Novus Energy Technologies (Novus), Carus Corporation (Carus), and Applied Membrane Technology, Inc. (AMT) to develop an innovative Geothermal ThermoElectric Generation (G-TEG) system specially designed to both generate electricity and extract high-value lithium (Li) from low-temperature geothermal brines. The process combined five modular technologies including – silica removal, nanofiltration (NF), membrane distillation (MD), Mn-oxide sorbent for Li recovery, and TEG. This project provides a proof of concept for each of these technologies.

The first step in the process is silica precipitation through metal addition and pH adjustment to prevent downstream scaling in membrane processes. Next, the geothermal brine is concentrated with the first of a two stage MD system. The first stage MD system is made of a high-temperature material to withstand geothermal brine temperatures up to 150 °C. The first stage MD is integrated with a G-TEG module for simultaneous energy generation. The release of energy from the MD permeate drives heat transfer across the TE module, producing electricity. The first stage MD concentrate is then treated utilizing an NF system to remove  $\text{Ca}^{2+}$  and  $\text{Mg}^{2+}$ . The NF concentrate will be disposed in the well by reinjection. The NF permeate undergoes concentration in a second stage of MD (polymeric material) to further concentrate Li in the NF permeate and enhance the efficiency of the downstream Li recovery process utilizing a Mn-oxide sorbent. Permeate from both the stages of the MD can be beneficially utilized as the permeates will contain less contaminants than the feed water. The concentrated geothermal brines are then contacted with the Mn-oxide sorbent. After Li from the geothermal brine is adsorbed on the sorbent, HCl is then utilized to regenerate the sorbent and recover the Li.

The research and development project showed that the Si removal goal (>80%) could be achieved by increasing the pH of the brine and adding  $\text{Fe}^{3+}$  under several scenarios. The NF was also successful in achieving significant  $\text{Ca}^{2+}$  and  $\text{Mg}^{2+}$  removal (~80%) while retaining most Li in the permeate for high strength brines. MD experiments showed that geothermal brines could be significantly concentrated with little fouling due to pre-treatment.

**2.0 TABLE OF CONTENTS**

**1.0 EXECUTIVE SUMMARY .....2**

**2.0 TABLE OF CONTENTS .....3**

**3.0 INTRODUCTION.....4**

**4.0 SiO<sub>2</sub> PRECIPITATION.....6**

    4.1 Methods and Materials .....6

    4.2 Results and Discussion .....7

**5.0 NANOFILTRATION. ....12**

    5.1 Methods and Materials .....12

    5.2 Results and Discussion.....14

**6.0 MEMBRANE DISTILLATION. ....17**

    6.1. Methods and Materials .....17

    6.2. Results and Discussions .....19

**7.0 Mn-OXIDE SORBENT .....25**

    7.1. Methods and Materials .....25

    7.2. Results and Discussions .....26

**8.0 THERMOELECTRIC POWER GENERATION SYSTEM. ....34**

    8.1. Thermoelectric Material Development .....34

    8.2. Thermoelectric Module Fabrication Results .....35

    8.3. Integrated Membrane Distillation .....37

**9.0 TECHNICAL AND ECONOMIC ANALYSIS.....42**

**10.0 CONCLUSIONS. ....50**

**11.0 REFERENCES.....51**

### 3.0 INTRODUCTION

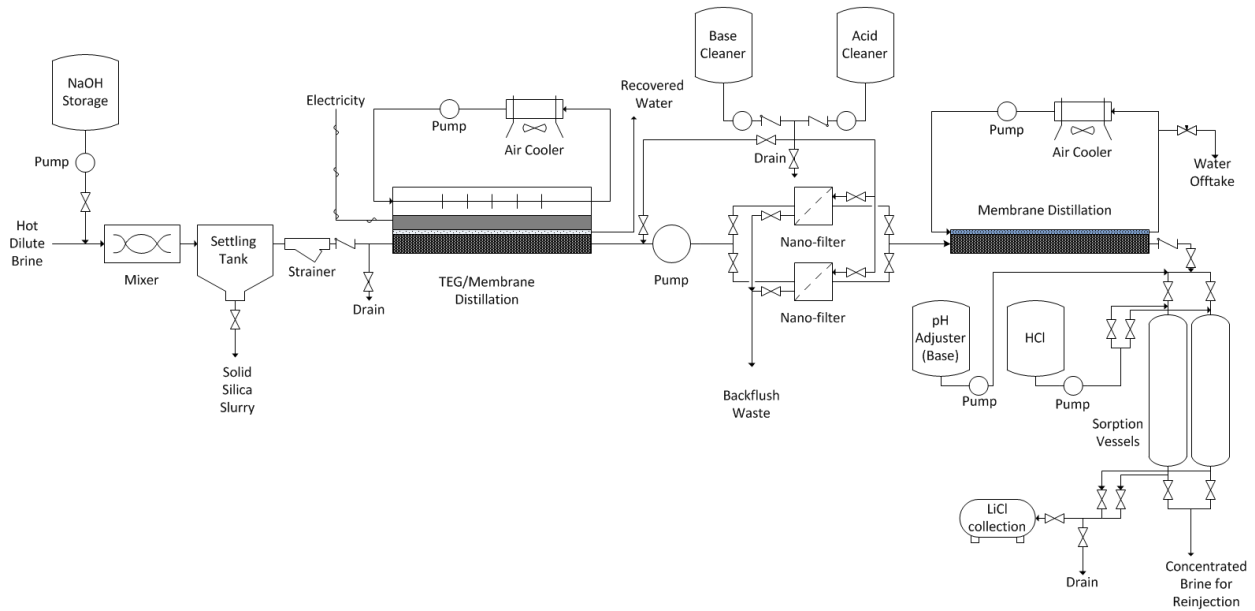
Southern Research Institute (Southern), with partners Novus Energy Technologies (Novus), Carus Corporation (Carus), and Applied Membrane Technology, Inc. (AMT) worked to develop an innovative Geothermal ThermoElectric Generation (G-TEG) system specially designed to both generate electricity and extract high-value Li from low-temperature geothermal brines (<150 °C). The process combined five modular technologies including – silica removal, nanofiltration (NF), membrane distillation (MD), Mn-oxide sorbent for Li recovery, and TEG. This project provides a proof of concept for each of these technologies.

Figure 3.1 shows a process flow diagram for the system. The first step is silica removal through inorganic metal addition and pH adjustment to prevent scaling in downstream membrane processes. In a revised concept for the project, we include ultrafiltration with ceramic membranes to remove the precipitated silica and other solids instead of a settling tank. Next, the geothermal brine is concentrated with the first of a two-stage MD system. The first stage MD system is made of a high-temperature material to withstand geothermal brine temperatures up to 150 °C. The first stage MD is integrated with a G-TEG module for simultaneous energy generation and concentration. Water vapor passing through the membrane will condense on contact with the colder thermoelectric generator (TEG), which will harness the latent heat given off by the water vapor to produce electricity and reject waste heat to an evaporative chilled cooling loop. The first stage MD is only designed to concentrate the geothermal brine by approximately 15%; hence, fouling should be minimal in this first stage system. The release of energy from the MD permeate drives heat transfer across the TE module, producing electricity. The remaining brine passing through the first stage MD is then treated utilizing a NF system to remove  $\text{Ca}^{2+}$  and  $\text{Mg}^{2+}$ . The NF concentrate will be sent back to the well for reinjection. The NF permeate undergoes concentration in a second stage of MD (polymeric material) to further concentrate Li in the NF permeate and enhance the efficiency of the downstream Li recovery process utilizing a Mn-oxide sorbent. Permeate from both the stages of the MD can be beneficially utilized as both permeates will contain significantly less contaminants than the original geothermal brine. The concentrated geothermal brines are then contacted with the Mn-oxide sorbent. After Li from the geothermal brine is adsorbed on the sorbent, HCl is then utilized to regenerate the sorbent and recover Li.

The goals of this project were to: (1) develop a thermoelectric based power generation system that can economically produce baseload renewable electricity from low-temperature

geothermal brines, and (2) to extract high-value Li from the geothermal brine to provide additional system revenue as an untapped supply for this high demand resource.

The modular system development for the project was divided into six (6) sub-sections – silica removal, nano-filtration, membrane distillation, Mn-oxide sorption, thermo-electric generator, and pro-forma model. This project includes proof of concept evaluations of the technologies listed above.



**Figure 3.1.** Process flow diagram of integrated system.

## 4.0 Silica Removal

Silica removal from the geothermal brine is necessary to avoid fouling and scaling in the downstream membrane processes. Silica can impede membrane operations through fouling of the membrane [1].

Previous researchers have reported that increasing pH can increase silica removal from geothermal brines through increasing the degree of ionization of and promoting the oligomerization of silicate ion thereby promoting removal [2]. Note that the exact mechanism by which silica is removed has never been properly evaluated. Multi-valent ions such as  $\text{Ca}^{2+}$ ,  $\text{Mg}^{2+}$ ,  $\text{Fe}^{3+}$ , etc. have been shown to promote silica removal through acting as “bridging ions between silica surface and silicic acid ions” [2]. This process can promote polymer formation and therefore silica removal [2]. Silica could potentially be removed with precipitation of  $\text{Mg}(\text{OH})_2$  and other Mg-precipitates at higher pH. Addition of several metals such as  $\text{Ca}^{2+}$  and  $\text{Fe}^{3+}$  were attempted in the study coupled with pH increase. A summary of the  $\text{Fe}^{3+}$  results are in this section.

### 4.1 *Methods and Materials*

Experiments were conducted by increasing the pH of simulated geothermal brines with NaOH and  $\text{Fe}^{3+}$  ( $\text{FeCl}_3$ ) in high density polyethylene (HDPE) containers. The brines were made with addition of  $\text{Fe}^{3+}$  at varied Fe/Si molar ratios. The Fe/Si ratios were based on the total amount of each element added to the solution. Hence, elements could precipitate out of the dissolved phase changing the dissolved ratios somewhat from the ratios added and shown on the graph. Temperatures were also varied in some experiments utilizing a water bath. The reaction time for the experiments was generally 30 minutes. NaOH (and  $\text{HNO}_3$  as needed) was also added to maintain the approximate target pH level throughout the experiment. The volume change from the acid or base addition was assumed to be insignificant and not taken into account. After reaction, a sample of the fluid was filtered (0.45  $\mu\text{m}$  filters) and analyzed for Si content utilizing inductively coupled plasma-mass spectrometry (ICP-MS). The original simulated brine was also evaluated for Si. Table 4.1 shows the measured dissolved composition of the simulated brines produced with  $\text{Cl}^-$  and  $\text{SO}_4^{2-}$  salts that were utilized in the experiments as measured by ICP-MS right before the experiments began. The initial brine pH was generally in the range of 5.5 to 6.5.

**Table 4.1.** Simulated Brine Formulas for Silica Precipitation Experiment.

Component	Low Strength Brine Concentration (mg/L)	High Strength Brine Concentration (mg/L)
Si	7-13	70-113
Na	505-1,483	2,591-3,162
K	243-253	672-688
Mg	16-21	83-216
Ca	20-31	441-446

**4.2 Results and Discussion**

Figures 4.1 through 4.4 show the results for the silica removal experiments at pH values of 9.0 and 10.5. The removal is calculated based on the Si concentration removed from the dissolved phase. The experiments were conducted at two temperatures approximately 50 and 80 °C. The results indicate that no Fe<sup>3+</sup> addition is necessary to meet the 80% Si removal goal for high strength brines under any of the scenarios likely due to silica adsorption to Mg-OH precipitates at higher pH. Much of the Mg was removed in the experiments. The pH adjustment alone meets the goal.

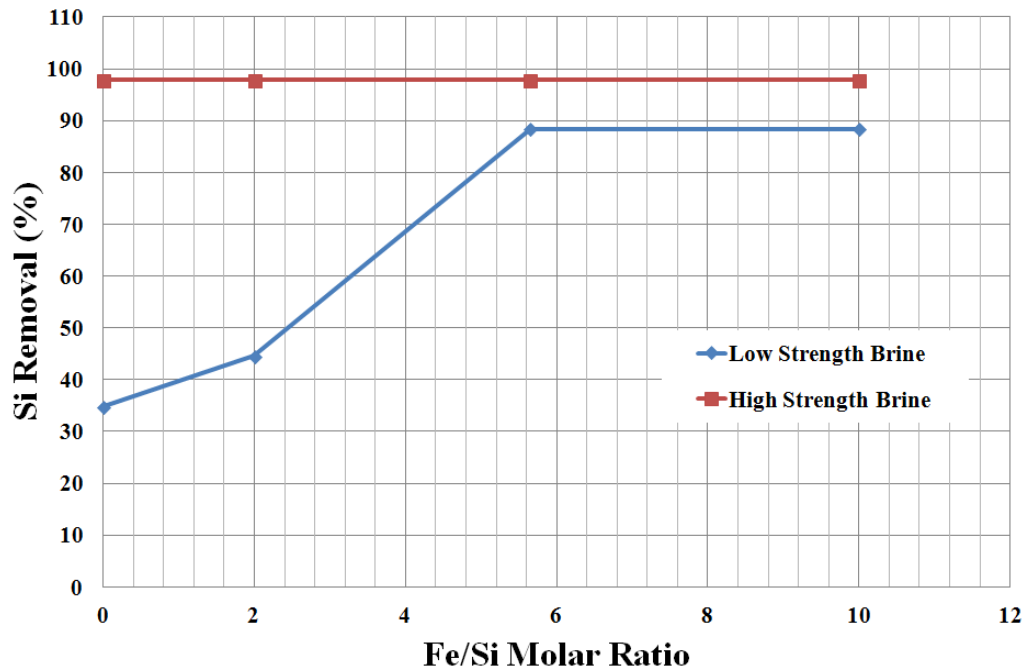


**Figure 4.1.** Si removal results for Fe<sup>3+</sup> addition with the pH maintained at 9.0 and temperature maintained at 80 °C.

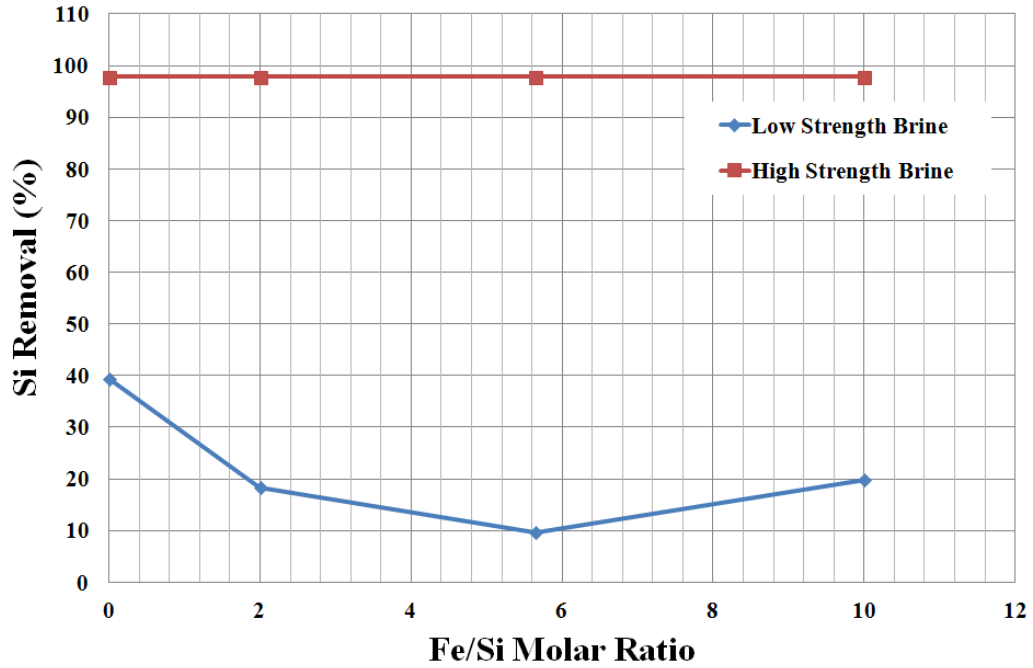


**Figure 4.2.** Si removal results for Fe<sup>3+</sup> addition with the pH maintained at 10.5 and temperature maintained at 80 °C.

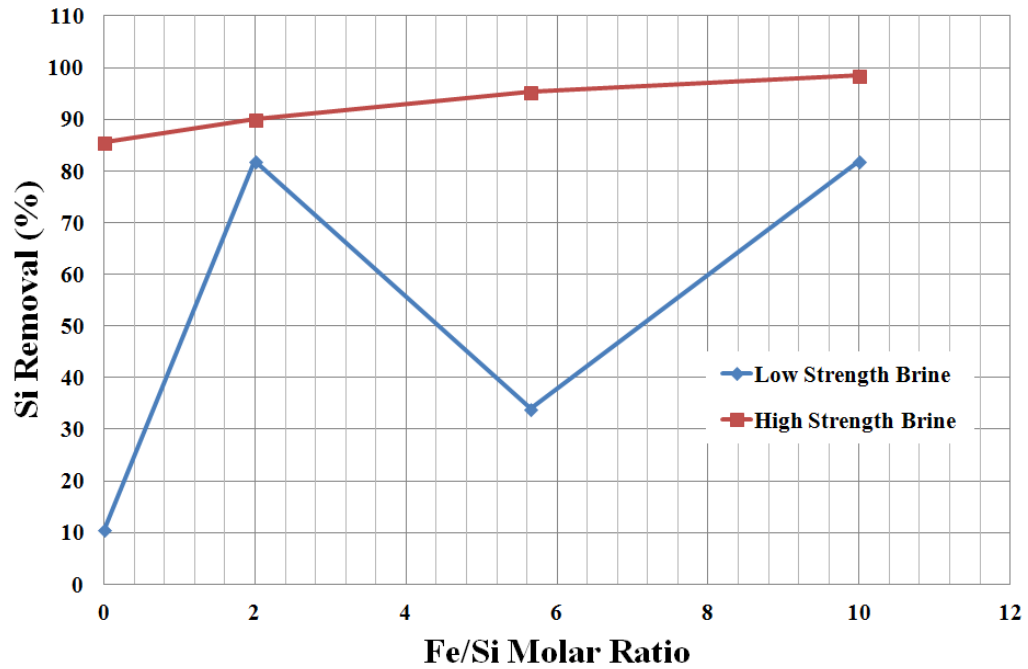


**Figure 4.3.** Si removal results for Fe<sup>3+</sup> addition with the pH maintained at 9.0 and temperature maintained at 50 °C.

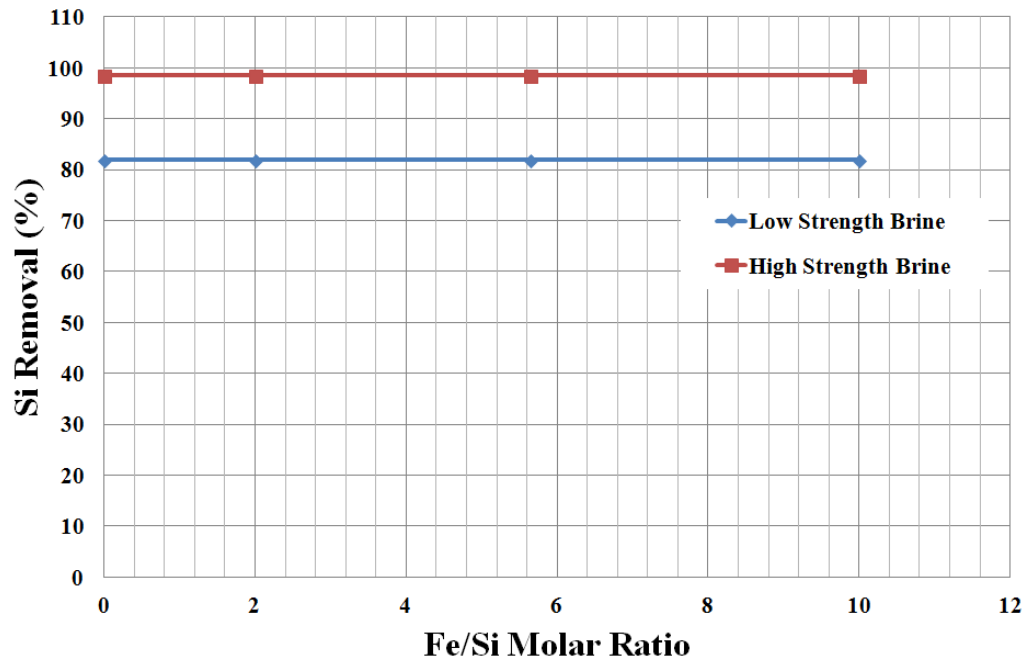


**Figure 4.4.** Si removal results for  $\text{Fe}^{3+}$  addition with the pH maintained at 10.5 and temperature maintained at 50 °C.

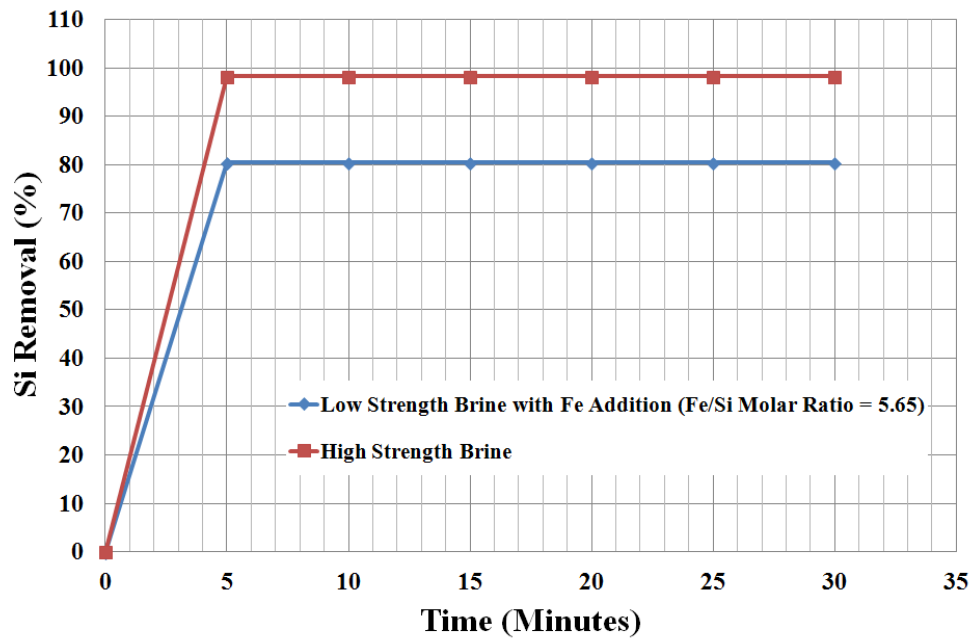
$\text{Fe}^{3+}$  addition can enhance Si removal for the low strength brines at pH = 9.0 for both temperatures (50 °C and 80 °C) as shown in Figures 4.1 and 4.3. While at pH = 10.5 and temperature = 80 °C,  $\text{Fe}^{3+}$  addition decreased Si removal as shown in Figure 4.2. At pH = 10.5 and temperature = 50 °C,  $\text{Fe}^{3+}$  addition had no impact and pH adjustment alone reached the 80% removal goal.

Figure 4.5 shows a kinetic experiment conducted for the most favorable Si precipitation conditions (pH = 9.0, temperature = 80 °C, and Fe/Si molar ratio = 5.65 for low strength brine, no metal addition for high strength brine). The results show that the Si removal reactions occur very rapidly (<5 minutes). Hence, little time will be required for the process in a full scale application. Time 0 was defined as before any adjustments were made to the solutions (pH or Fe/Si addition).

Figures 4.6 through 4.8 show the results for the experiment when the pH is only adjusted to 6.0, 7.0, and 8.0. The results show that the silica removal process will reach desired levels at pH 6.0 and 7.0 for the high strength brine when a large amount of  $\text{Fe}^{3+}$  (Fe/Si molar ratio = 5.65) is added. At pH 8.0, less  $\text{Fe}^{3+}$  (Fe/Si molar ratio ~ 2) has to be added to the high strength brine to successfully remove silica as shown in Figure 4.8.

In summation, the silica removal strategy should be based on the chemical composition and temperature of the geothermal brine. The particular brine may require only pH adjustment plus

metal addition. It is believed that the produced solids could likely be removed efficiently through ultrafiltration.



**Figure 4.5.** Kinetics of Si removal with Fe(+III) addition. pH maintained at 9.0 and temperature maintained at 80 °C. Fe/Si molar ratio = 5.65 for low strength brine.

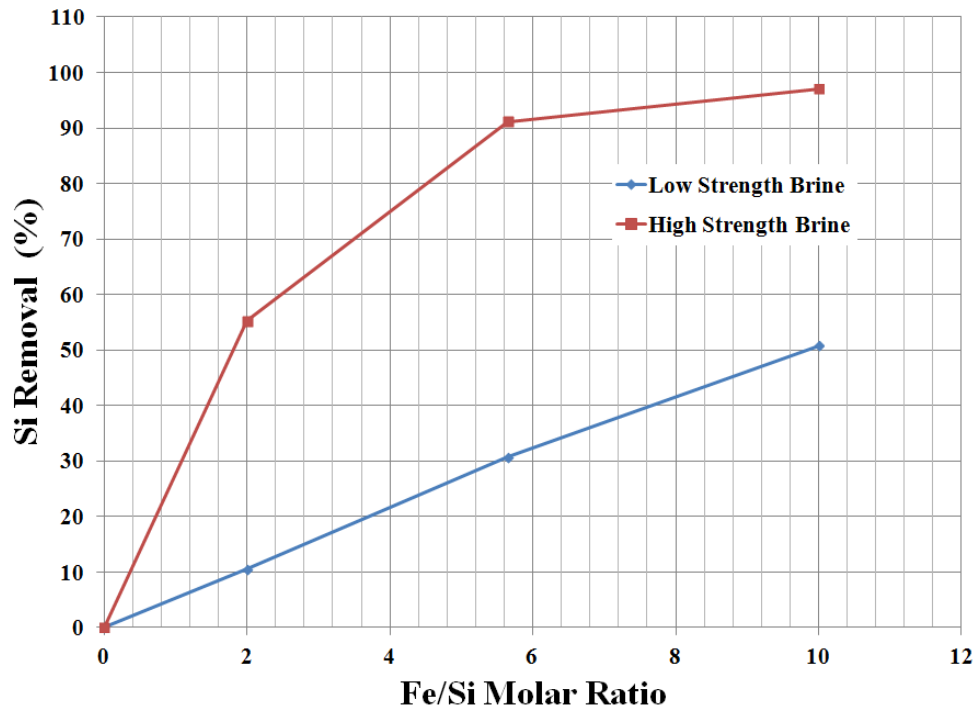


**Figure 4.6.** Si removal results for Fe<sup>3+</sup> addition with the pH maintained at 6.0 and temperature maintained at 80 °C.

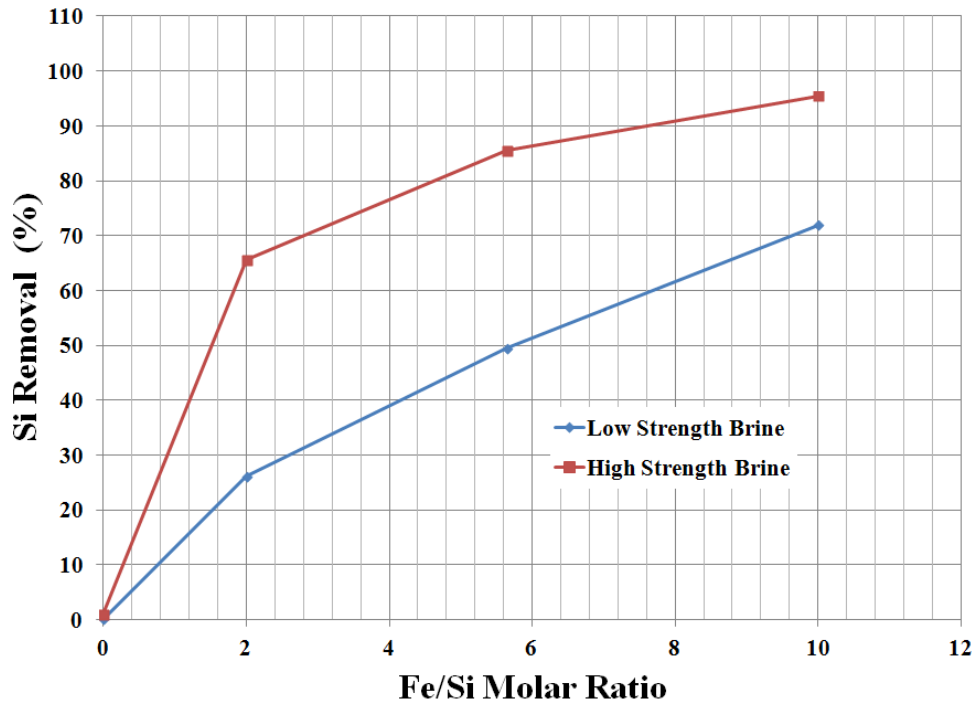


**Figure 4.7.** Si removal results for  $\text{Fe}^{3+}$  addition with the pH maintained at 7.0 and temperature maintained at 80 °C.

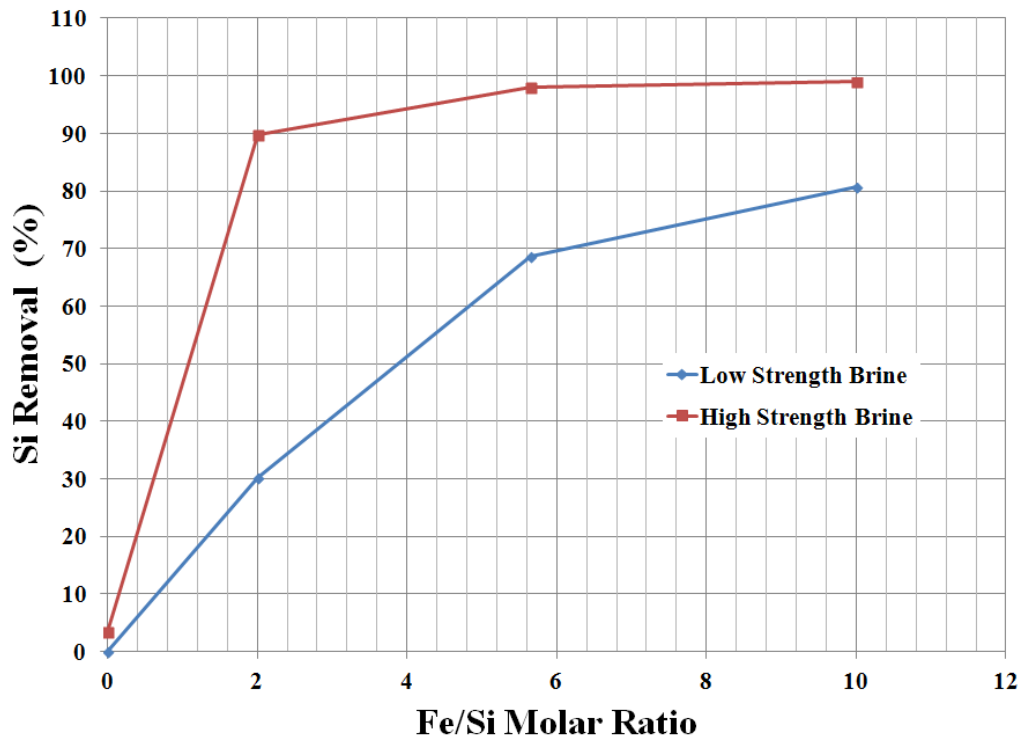


**Figure 4.8.** Si removal results for  $\text{Fe}^{3+}$  addition with the pH maintained at 8.0 and temperature maintained at 80 °C.

## 5.0 NANOFILTRATION

Nanofiltration (NF) is an intermediate pressure driven membrane process which resides between ultrafiltration (UF) and reverse osmosis (RO) and has typically been utilized to in treatment strategies for seawater to provide drinking water purposes [3, 4]. NF rejects solutes mainly by two mechanisms – electrostatic attraction between charged dissolved species and the surface of the membrane and size exclusion of the solute by the membrane [3, 5, 6].

NF generally requires smaller pumps (lower pressure) and requires less energy utilization and pre-treatment chemicals than RO [7]. Because of its ability to reject divalent ions, especially including  $\text{Ca}^{2+}$  and  $\text{Mg}^{2+}$ , NF has been utilized upstream of RO in order to prevent membrane fouling. NF is typically applied to feedwaters with TDS ranges of 5,000 to 25,000 mg/L [4].

NF is an optimum technology to separate Li from divalent ions. Li can pass through NF due to the element being monovalent and its small size. Previous studies have shown NF effective in separating Li from multi-valent ions [8-10]. One study achieved a 85% separation between the  $\text{Mg}^{2+}$  and Li in a brine from a salt lake [8]. Li passes through to the permeate while the divalent ions are rejected at higher rates.

The purpose of the NF evaluation is to separate Li from the divalent ions  $\text{Ca}^{2+}$  and  $\text{Mg}^{2+}$ . These divalent ions are separated from the Li for the dual purpose of reducing the formation of minimally soluble salts which cause fouling in the downstream membrane distillation unit and also to prevent interference with the Li sorption process. Some of the more recent NF results are reviewed in this section.

### 5.1 *Methods and Materials*

A bench-scale batch NF system was utilized as shown in Figure 5.1. Simulated geothermal brines were added to the reservoir. Table 5.1 shows the composition of the simulated brines that were utilized in the experiments. The values in Table 5.1 are measured values. The brines utilized included low strength brine, high strength brine, and high strength brine with additional Si added. The low strength and high strength brine had unadjusted initial pH values that ranged from 7.2 to 7.4. The high strength brine with Si added was had it's pH adjusted to 5.0 prior to the experiment. The actual brines would likely contain less  $\text{Mg}^{2+}$  in reality compared to Table 5.1 due to it  $\text{Mg}^{2+}$  precipitation in the silica removal step. However, higher concentrations were included in the NF study in order to evaluate the effectiveness of the NF process to remove  $\text{Mg}^{2+}$ . The simulated

brines were processed through the NF until approximately 70% (actual 63.1-71.3%) of the feed was recovered as permeate. The reject from the NF is recycled back to the feed in the batch experiments. The pressure was generally maintained at approximately 200 psi. Temperature of the concentrate in the reservoir was not maintained or monitored, but it was noticed that the concentrate warmed some during the process.

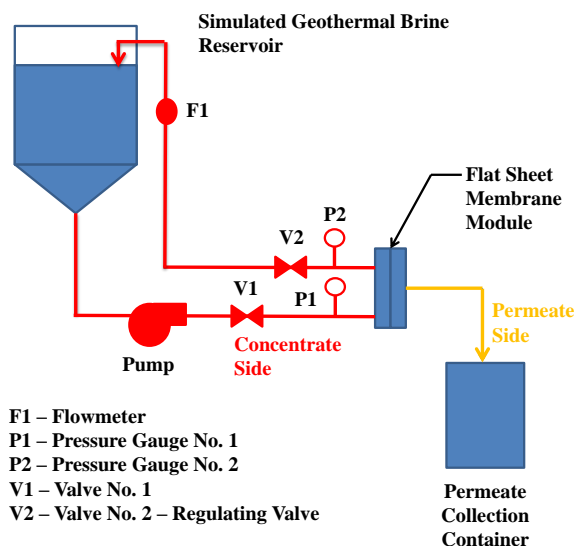


Figure 5.1. Approximate experimental NF configuration.

Table 5.1. Simulated feed geothermal brines composition.

Component	Low Strength Brine (mg/L)	High Strength Brines (mg/L)	High Strength Brine with Si (mg/L)
Ca	22	420	460
Cl	1,800	7,030	14,220
Li	1	20	22
Mg	13	60	230
Na	880	3,670	7,050
Si	2	0	12
SO <sub>4</sub>	63	380	400

Three samples are analyzed for each NF evaluation. The first sample is the feed simulated brine (before the experiment). The final permeate is analyzed following the end of the experiment. The concentrate, which is the simulated brine remaining in the feed tank following processing to a target 70% permeate recovery, is also analyzed. In the total project, the feed, permeate, and concentrate are analyzed utilizing ICP-MS to determine Ca<sup>2+</sup>, Li<sup>+</sup>, Mg<sup>2+</sup>, Na<sup>+</sup>, and Si concentrations; however, some samples were also analyzed for Cl<sup>-</sup>, SO<sub>4</sub><sup>2-</sup>, and Li<sup>+</sup> utilizing ion chromatography (IC).

Three NF membranes evaluated are shown in Table 5.2. The Table also shows the specifications for the membranes. The molecular weight cut-offs (MWCO) for the membrane varies from 100 to 500 Daltons. The MWCO is the lowest molecular weight in a solution that 90% of a solute will be rejected by the membrane [11].

**Table 5.2.** NF membranes utilized in experiments.

No.	Manufacturer	Type	Polymer	MWCO (Daltons)	MgSO <sub>4</sub> Rejection (%)
1	TriSep	TS80	Polyamide	~100-200	>99%
2	Snyder	NFX	Polyamide-	~150-300	99
3	Snyder	NFW	Polyamide-	~300-500	97

## 5.2 Results and Discussion

Figures 5.2 through 5.5 show the NF results. The rejection efficiency was calculated per equation 5.1.

$$\text{Rejection Efficiency} = \left[ 1 - \left( \frac{PM}{FM \times R} \right) \right] \times 100 \quad (5.1)$$

PM is the mass of component of interest in the permeate in grams at the end of the experiment. FM is the initial mass of the component of interest in the feed in grams. The feed is the simulated brine that is put in the reservoir before the experiment starts. R is the ratio of the recovered permeate volume (L) to the total feed volume (L).

The average flux for the entire batch scale experiments varied from 2.3x10<sup>-2</sup> – 4.1x10<sup>-2</sup> gpm/ft<sup>2</sup>, 2.4x10<sup>-2</sup> – 3.2x10<sup>-2</sup> gpm/ft<sup>2</sup>, and 1.5x10<sup>-2</sup> – 3.1x10<sup>-2</sup> gpm/ft<sup>2</sup> for the low strength brine, high strength brine, and high strength brine with Si, respectively. However, it is noted that the experiments were conducted in batch mode and as a result the feed became more concentrated

over time. Hence, the average flux for a continuous process would likely be significantly higher than the batch scale experiments.

Figure 5.2 shows that for the most important case, the high strength brines, low percentages of Li were removed from the simulated geothermal brines per Equation 5.1. It is unlikely that the technology would be applied to brines with low Li content due unfavorable economics associated with low Li recovery; hence, the high strength brine case is more important. For the high strength brine samples, <25% of Li was removed from the brine per Equation 5.1.

Figure 5.3 shows that utilizing a membrane with a midpoint MWCO of approximately 150 Daltons will remove approximately 80% of the  $\text{Ca}^{2+}$  and  $\text{Mg}^{2+}$  from high strength geothermal brines. Figure 5.4 shows the removals for  $\text{Cl}^-$  and  $\text{SO}_4^{2-}$ . The results for the high strength brine show that a large percentage of the  $\text{SO}_4^{2-}$  is removed (>90% at midpoint MWCO = 225 Daltons). As expected, little  $\text{Cl}^-$  is removed by the NF membrane.

The results of the project indicate that NF is capable of successfully separating Li from divalent ions and meeting the requirements of the technology. Additional testing for this process is necessary, but NF shows excellent promise for the proposed application. NF provides excellent pre-treatment upstream of the polymeric MD to reduce scaling in this stage of the MD.

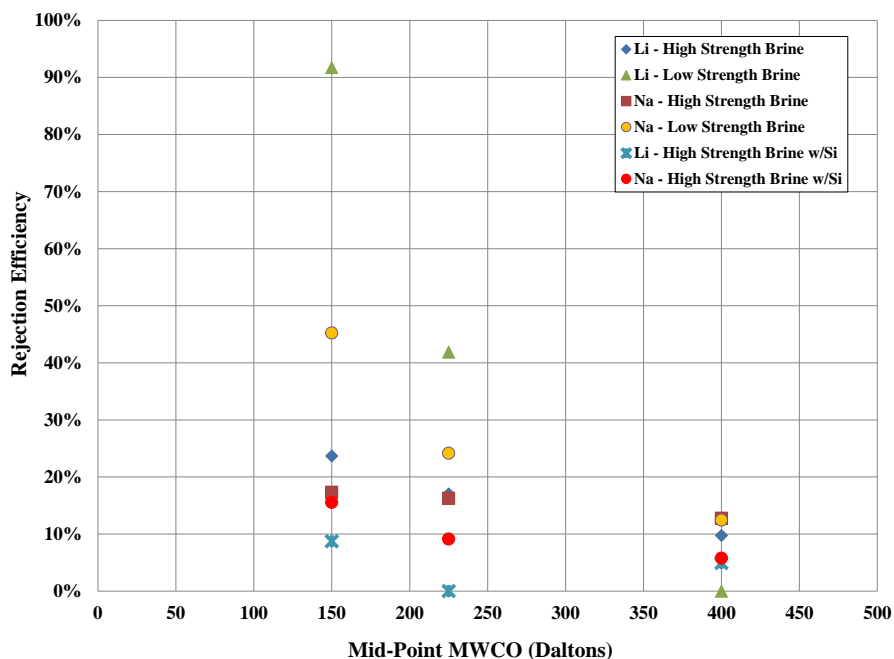


Figure 5.2.  $\text{Li}^+$  and  $\text{Na}^+$  rejection efficiency.

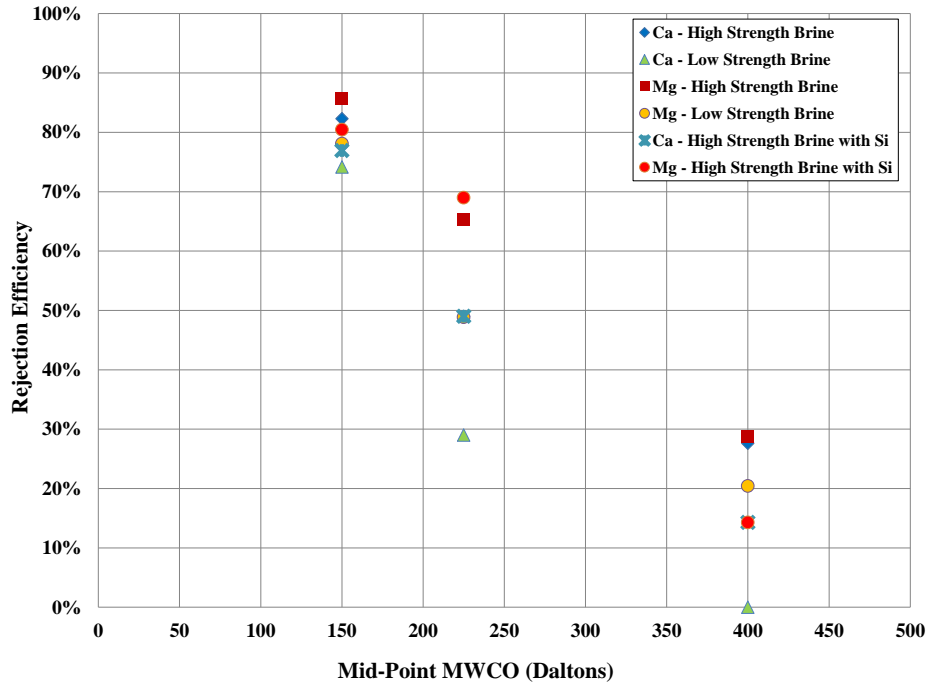


Figure 5.3. Ca<sup>2+</sup> and Mg<sup>2+</sup> rejection efficiency.

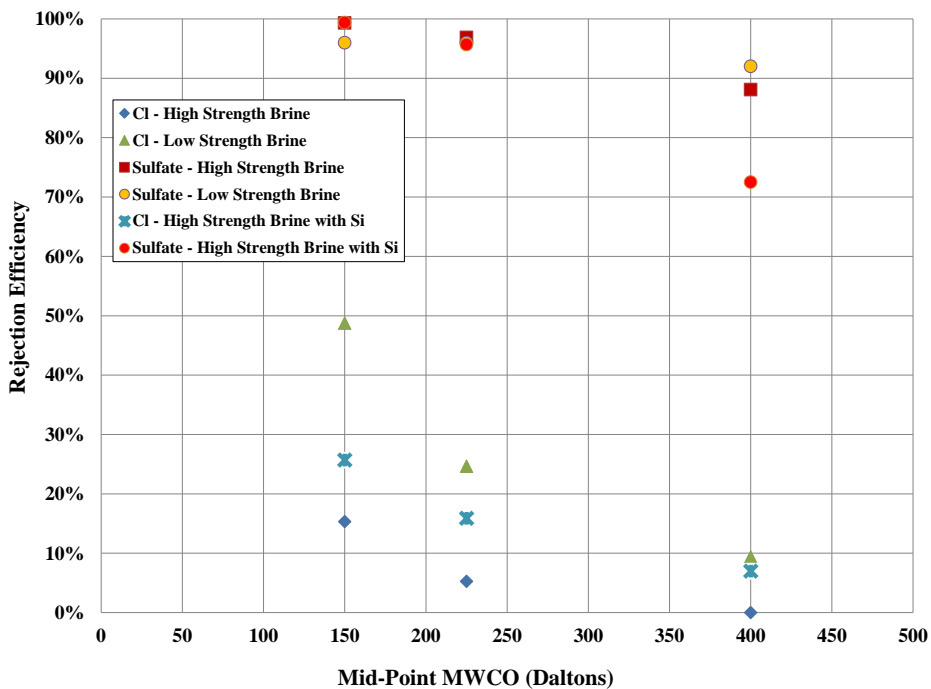


Figure 5.4. Cl<sup>-</sup> and SO<sub>4</sub><sup>2-</sup> rejection efficiency.

## 6.0 MEMBRANE DISTILLATION

Membrane distillation (MD) is a process that can separate dissolved species from water through vapor pressure differences between the permeate and the concentrate [12]. A hydrophobic membrane separates the permeate from the concentrate in this system and no water can enter the membrane pores due to high surface tension [12]. The only way that water can be transferred from the concentrate to the permeate side is through water vapor [12]. Temperature differences between the concentrate and permeate can be utilized to maintain the required vapor pressure gradient [13-18]. MD can be combined with waste heat to drive the temperature gradient. Although a significant heat input is required, brine desalination has been accomplished even at temperatures  $<50\text{ }^{\circ}\text{C}$  [13]. The distillate produced by MD is generally of good quality. MD is utilized in this process to both concentrate the Li in the brine and also recover water. Experiments were conducted utilizing simulated low temperature geothermal brines.

### 6.1 *Methods and Materials*

Figure 6.1 shows a simplified diagram of the MD system. Figure 6.2 shows a drawing of the MD membrane. The MD's microporous, hydrophobic membranes are composed of polypropylene fibers having a thin hydrophobic microporous coating of a silicone-fluoropolymer plasma polymerized on the fiber outside diameter on the hot brine side to prevent pore wetting. Further, the  $330\text{ }\mu\text{m}$  inner diameter hydrophobic porous hollow fibers have relatively thick walls ( $150\text{ }\mu\text{m}$ ), high porosity, and larger diameter ( $630\text{ }\mu\text{m}$  outer diameter).

Simulated brine solutions at three (3) different strengths – low, medium and high were prepared to conduct MD concentration tests.

The brine solution entering the MD column was maintained at a temperature in the general range of  $115\text{-}165\text{ }^{\circ}\text{F}$  ( $46\text{-}74\text{ }^{\circ}\text{C}$ ) using a coil heater and heat exchanger. The brine was recirculated through the column at a constant rate of 1 GPM. Distillate was recirculated through the membrane at a constant rate of one 0.26 GPM and at general approximate temperature range of  $75\text{-}90\text{ }^{\circ}\text{F}$  ( $24\text{-}32\text{ }^{\circ}\text{C}$ ) entering the membrane. The distillate was cooled by flowing cold tap water through the other side of the heat exchanger shown in Figure 6.1. The MD pilot unit was run a minimum of six (6) hours on each brine solution. Two (2) sets of brine and distillate samples were collected and analyzed for the composition to evaluate the efficiency of the MD system. High strength brine was run for a longer duration ( $\sim 10$  hours) and three (3) sets were collected. Volumes of brine and

distillate were measured at the end of each test run to calculate average flux of the system. Samples were analyzed utilizing ICP-MS for metals and IC for anions.

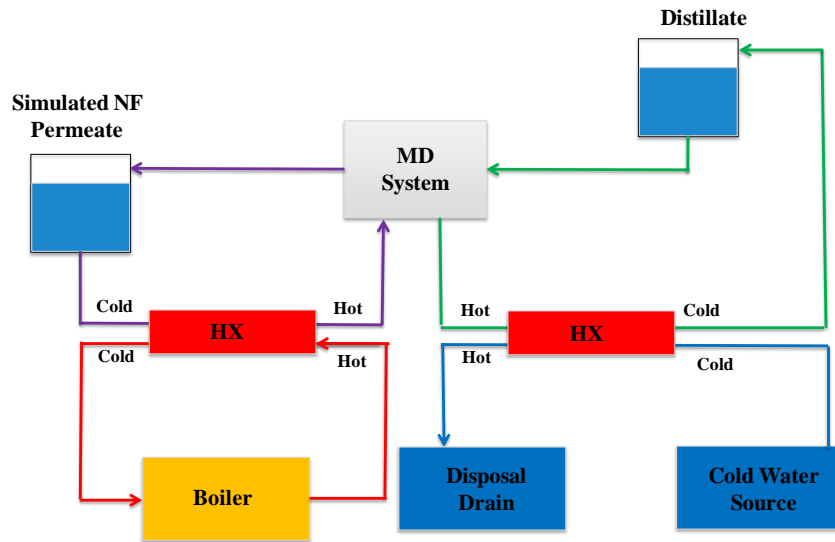


Figure 6.1. Simplified approximate MD system diagram.

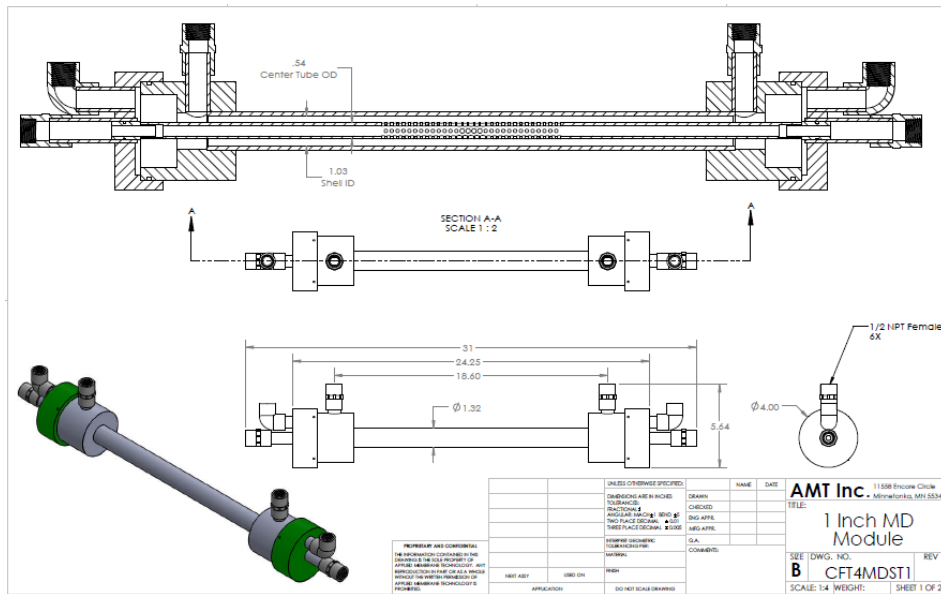


Figure 6.2. MD module.

Long-term performance of the MD system was evaluated by running the system on simulated high strength brine solution for a longer duration. The system was run for a total duration of 87.25 hours. High strength brine solution was prepared daily and added to the brine tank with pre-concentrated brine. Volume of the distillate collected at the end of each day operation was measured to calculate daily average flux rate. The system was not cleaned during the evaluation. Brine and distillate samples were collected at end of the test and analyzed to evaluate the efficiency of MD system to concentrate the geothermal brines.

## **6.2 Results and Discussion**

Figures 6.3 through 6.5 show the results of the MD experiments for the low strength, medium strength, and high strength simulated geothermal brines with values based on chemical analysis. Based on  $Cl^-$ , the 7.47 cycles of concentration were achieved for the high strength brine test. Some additional MD optimization is possible to maximize the TDS in the final concentrated brine.

Figure 6.6 shows the fate of the chemical components during the MD test. The results show that Li was rejected and remained in the brine. Figure 6.7 shows the average flux achieved during the MD tests. As expected, the highest flux was achieved for the low strength brine.

Results from the long term evaluation of the MD system indicated an average flux of  $5.33 \times 10^{-3}$  gpm/ft<sup>2</sup> over a total operation time of 87.5 hrs. The feed for the brine utilized in the long-term evaluation was prepared in the same manner as that for the high strength brine in Figure 6.5. A total volume of 45.3 gallons of distillate was collected from this test. Composition of brine, concentrate and distillate collected are shown in the Table 6.2. The results indicate that approximately 36 cycles of concentration were achieved based on  $Cl^-$ . The results also show that Li was not lost to the permeate and remained in the MD concentrate.

Average flux rates were calculated at end of each day operation irrespective of length of operation to evaluate the variation in the system throughput. The flux rate dropped initially but stayed consistent throughout the duration of the test. Variation in the flux rates is shown in Figure 6.8.

The results indicate that the system maintained a significant flux rate without scaling over a long term test. The overall results from the project can significantly concentrate geothermal brines without significant loss of Li, which improves the economics of the process. The upstream measures taken to decrease the potential for fouling (silica removal and NF) serve to maintain the integrity and performance of the membrane and MD system for long-term of operation.

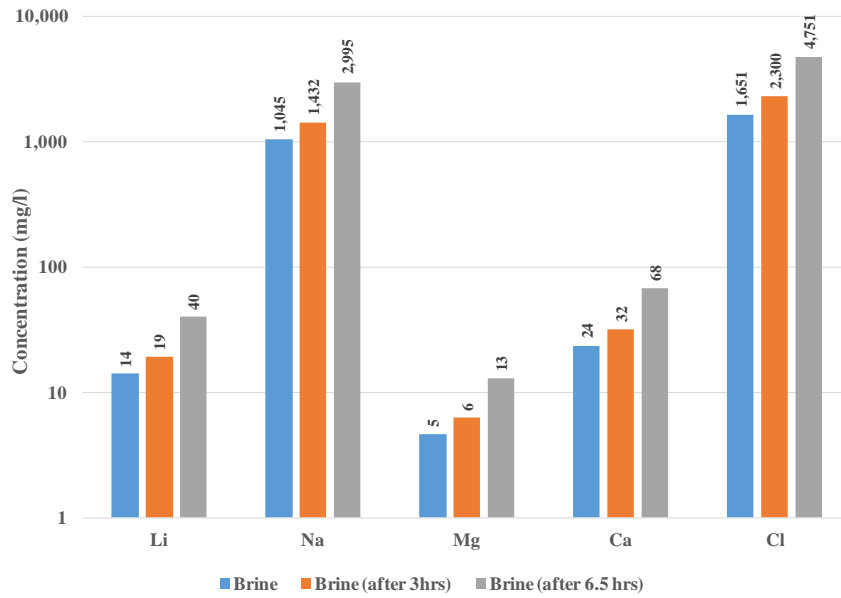


Figure 6.3. Low strength brine MD experiment.

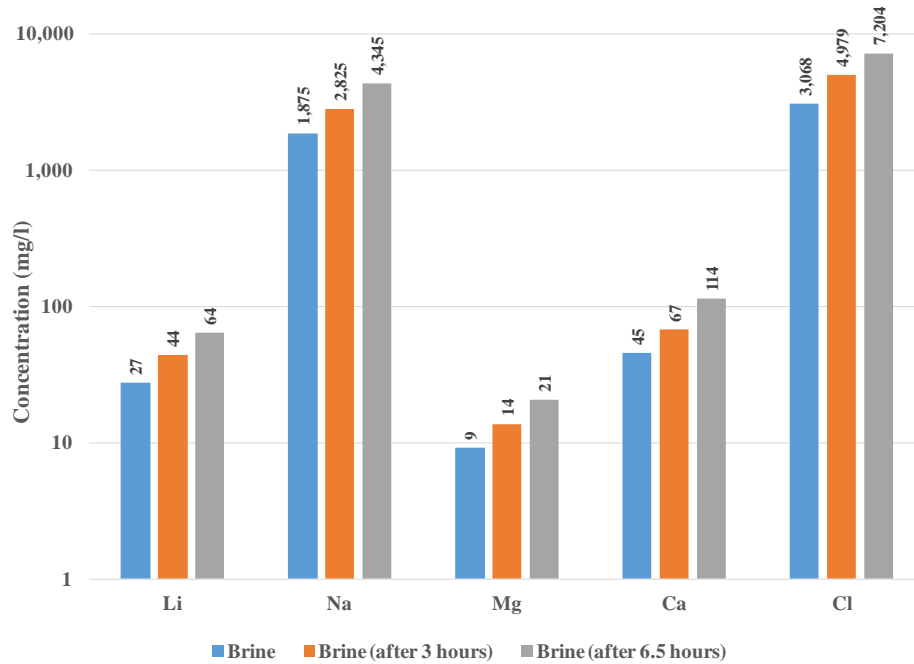


Figure 6.4. Medium strength brine MD experiment.

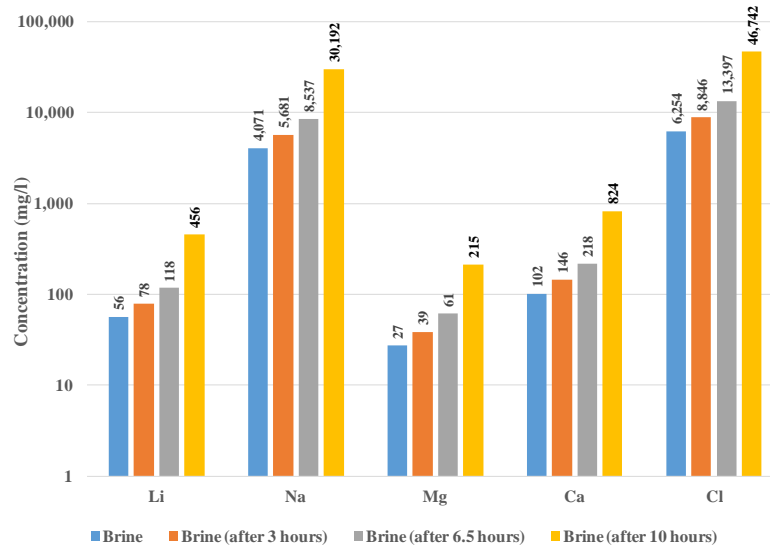
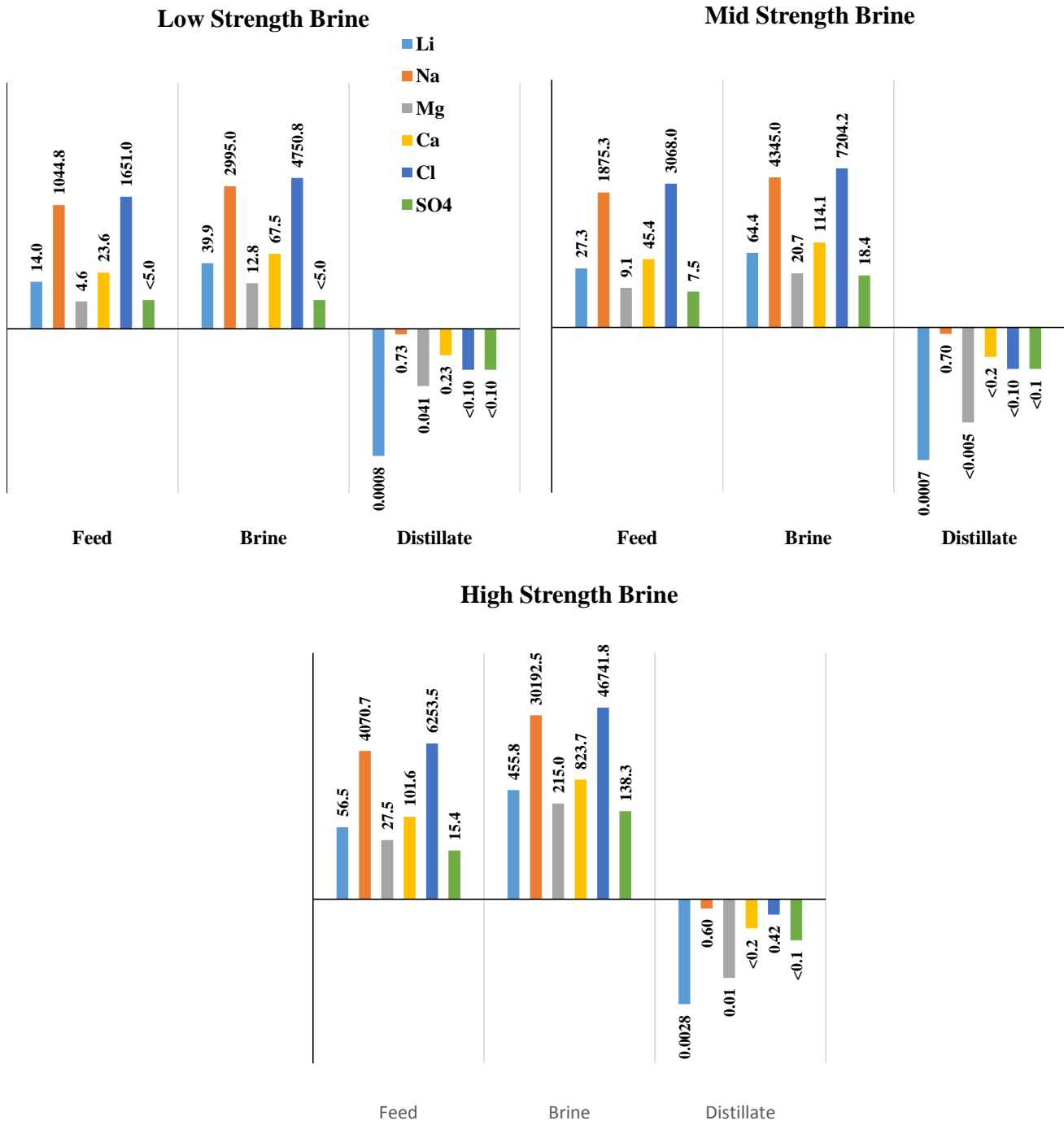
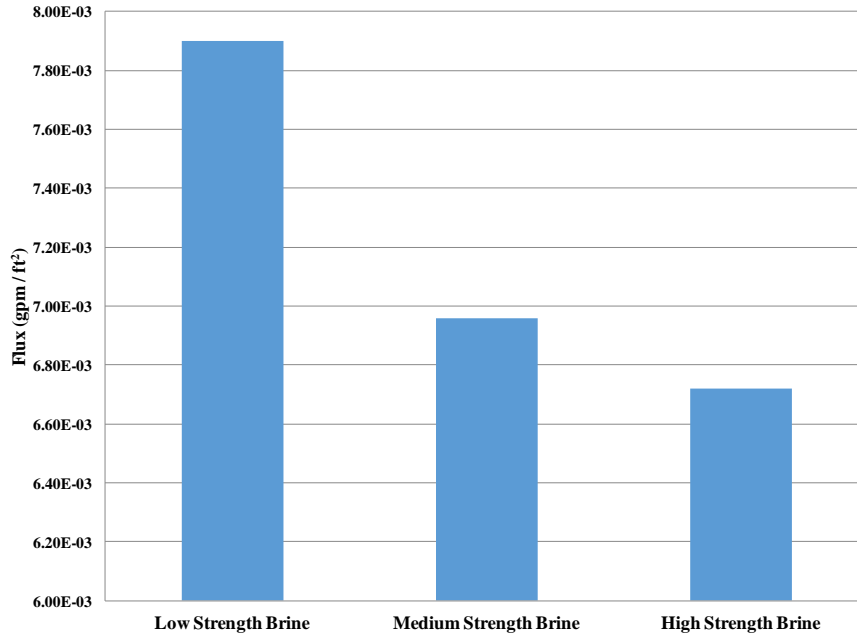


Figure 6.5. High strength brine MD experiment.



**Figure 6.6** Fate of Components in MD Experiment. Concentration in mg/L. Graphs are in Log scale.



**Figure 6.7.** Flux under different strength brine conditions.

**Table 6.1.** Longterm MD evaluation.

<b>Component</b>	<b>Concentrate (mg/L)</b>	<b>Distillate (mg/L)</b>
<b>Ca</b>	2,363	<11
<b>Cl</b>	129,818	<5
<b>Li</b>	1,216	<0.0028
<b>Mg</b>	428	1.2
<b>Na</b>	79,165	<2.75
<b>SO<sub>4</sub></b>	403	<5.0

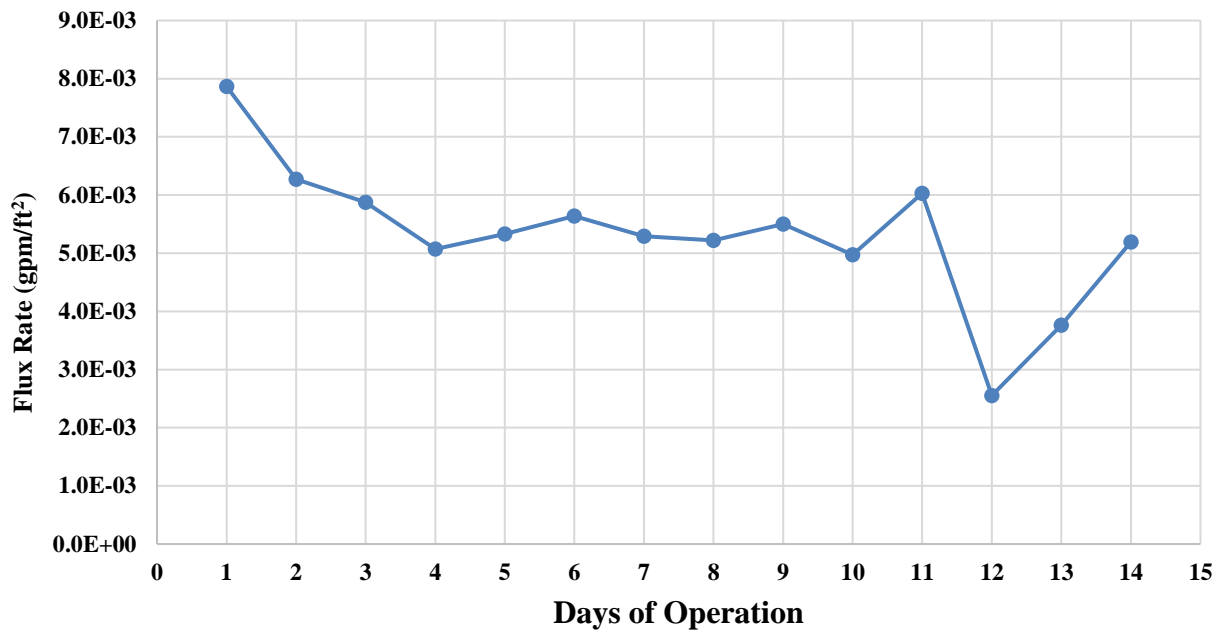


Figure 6.8. MD flux during long term evaluation.

## **7.0 Mn-OXIDE SORBENT**

Typical Li recovery methods include “ion exchange (adsorption), organic solvent extraction, and co-precipitation”[19]. Ion exchange methods have been shown to be appropriate for recovering Li from brines with some inorganic materials have been shown to selectively uptake  $\text{Li}^+$  and  $\text{H}^+$  into their pore structures [20]. Spinel forms of Li-Mn oxides have shown significant potential for recovering Li from aqueous streams and can be utilized as an ion sieve [21]. These spinel Li-Mn-oxide sorbents have very large pore structures and a large number of active sites for sorption which make them applicable for Li recovery [21].

Shi et al. demonstrated good uptake of Li onto  $\text{H}_{1.6}\text{Mn}_{1.6}\text{O}_4$  prepared from  $\text{Li}_{1.6}\text{Mn}_{1.6}\text{O}_4$  with a maximum uptake capacity of 27.15 mg/g sorbent from a brine at a temperature of 50 °C [21]. Shi et al.’s preparation of the sorbent included a pickling process only resulted in a Mn loss of 2.5% which is promising sign for the long term stability of the sorbent [21].  $\text{Mg}^{2+}$ ,  $\text{Na}^+$ , and  $\text{K}^+$  had a slight had a negative impact, although small on the effectiveness of the sorbent [21].

Sorption experiments were divided between Carus and Southern Research with Carus conducting most of the experiments. Four sorbents were evaluated in the project including in-situ formed nano hydrous manganese oxide (HMO) (Carus), purchased  $\text{LiMn}_2\text{O}_4$  (Carus), hydrothermally synthesized  $\text{LiMn}_2\text{O}_4$  (Carus), and synthesized  $\text{Li}_{1.6}\text{Mn}_{1.6}\text{O}_4$  (Southern Research).

### **7.1 Methods and Materials**

#### ***Carus***

For the Carus experiments, sorbents were contacted with distilled water and agitated utilizing a IKA T25 Digital Ultra Turrax (Guangzhou, China) set to a speed of 1,000 revolutions per minute (RPM). The liquid was separated from the sorbent utilizing 0.22 or 0.45  $\mu\text{m}$  filters. The temperature was varied in several of the experiments. Li measurements were made utilizing a Cole Palmer (Bunker, Connecticut) Four Elements Flame Photometer, Model 02655-15. It is noted that there is some uncertainty associated with the Li measurements made by Carus utilizing the flame photometer especially at high pH. The adsorption capacities measured with this instrument are included to show performance trends, not absolute values in this Chapter.

#### ***Southern Research***

For Southern Research experiments, solutions and sorbents were contacted in high density polyethylene (HDPE) containers. The containers were agitated by tumbling end over end for an

hour. The sorbent was then separated from the liquid utilizing ProWeigh Filters for TSS by Environmental Express (Charleston, South Carolina). Li measurements were analyzed by an Agilent (Santa Clara, California) 7700 inductively coupled plasma-mass spectrometer (ICP-MS). Additional details on the individual experiments are provided in the sections below.

## 7.2 Results and Discussion

The uptake of the Li onto sorbents was calculated utilizing equation 7.1.

$$Li \text{ Uptake} \left( \frac{mg \text{ Li}}{g \text{ sorbent}} \right) = \frac{Li \text{ Soln Mass} (t=0, \text{ mg}) - Li \text{ Soln Mass} (end, \text{ mg})}{\text{Solution Sorbent Dose} (g)} \quad (7.1)$$

### *nano-HMO (Carus)*

Carus attempted to extract Li from solution utilizing in-situ generated nano-HMO. HMO was generated in-situ so that maximum amount of active surface area was available for Li sorption. The sorbent was produced through the reaction in equation 7.2.



The first step included preparation of 100 mg/L of Li in distilled water. An equivalent concentration of  $Na_2S_2O_3$  was then added to the mixture and stirred for a minute. After mixing,  $KMnO_4$  was added at a stoichiometric amount. Samples were taken at time 0, 10, 30, 60, and 180 minutes. No Li uptake was observed even though Li:Mn ratio was increased. No Li uptake was observed under acidic and neutral conditions. However, increasing the pH did increase Li sorption. Figures 7.1 and 7.2 show the Li sorption to in-situ nano HMO with increasing pH. Generally, increasing the pH above 9.0 resulted in significant Li sorption to the HMO. However, for higher Li:Mn molar ratios (~4.0), no Li uptake was observed at higher pH.

### *Purchased $LiMn_2O_4$ (Carus)*

Carus purchased  $LiMn_2O_4$  for sorption experiments. 1.0 grams of  $LiMn_2O_4$  was dissolved in 100 mL of 1 M HCl to extract Li ions and replace with  $H^+$ . The solid was filtered, washed with distilled water, and dried overnight at 48 °C. The Mn was analyzed utilizing ICP emission spectrometry. As with nano-HMO, no sorption was observed under neutral conditions. However, as the pH increased, Li sorption was observed. Figure 7.3 shows the impact of increasing pH on the uptake of Li onto the purchased sorbent. Significant sorption was observed when the pH was increased above a pH of 9.0. Carus noted that the contact time to uptake Li on this sorbent was long which is why the results were not very promising for the purchased  $LiMn_2O_4$  sorbent.

**Hydrothermally Produced Spinel  $\text{LiMn}_2\text{O}_4$  (Carus)**

Carus also evaluated Li adsorption utilizing a hydrothermally produced spinel  $\text{LiMn}_2\text{O}_4$ . The method utilized for producing the sorbent was developed by Liddle et al. [22]. Carus produced the sorbent utilizing  $\text{KMnO}_4$ ,  $\text{LiOH}$ ,  $\text{C}_3\text{H}_8\text{O}$ , and  $\text{C}_3\text{H}_6\text{O}$  as follows: 13 mL of 0.1 M  $\text{LiOH}$  was reacted hydrothermally with 0.158 g of  $\text{KMnO}_4$  and 1.1 equivalents of reducing agents inside the 24 mL polytetrafluoroethylene (PTFE) high-pressure autoclave. The autoclave was heated to 180 °C at a rate of 10 °C per minute and the temperature was held at this temperature for five hours and then the autoclave was then allowed to cool overnight.

The sorbent was next separated from the liquid through filtration. The precipitates were then washed with distilled water and then dried in an oven overnight. The precipitates were digested and analyzed for Mn and K concentrations utilizing ICP emission spectra. The formula for the sorbent was expected to be  $\text{LiMn}_2\text{O}_4$ , but Carus did not analyze the Mn to active O ratio so the formula could be slightly different than  $\text{LiMn}_2\text{O}_4$ .

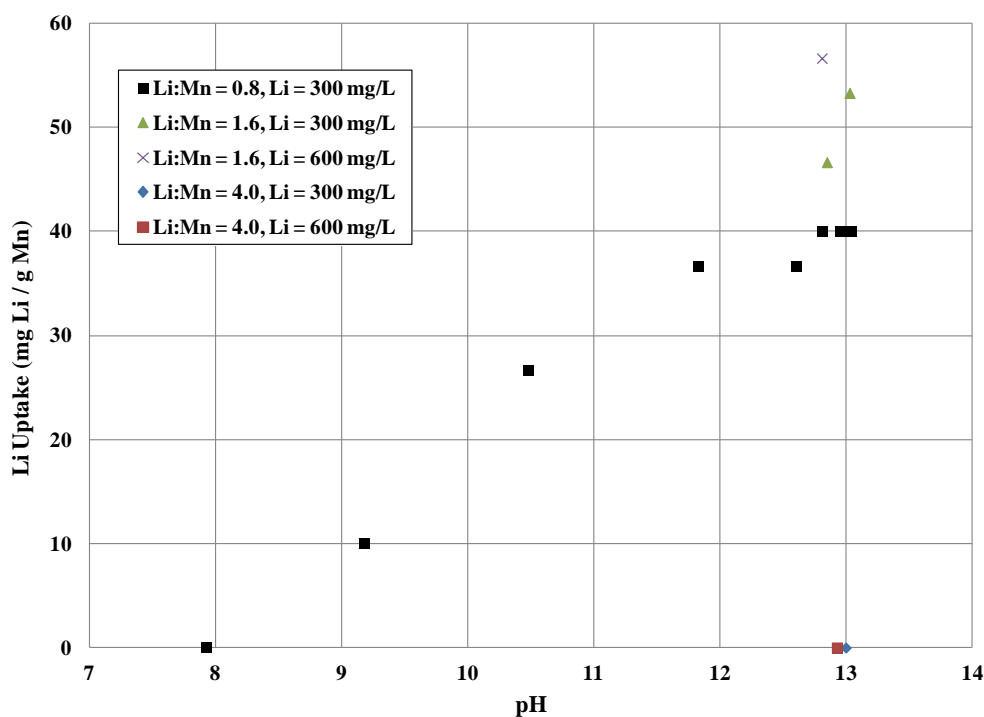


**Figure 7.1.** Li uptake on nano HMO. Li:Mn is on a mol:mol basis. Matrix is distilled water and the contact time = 1 hour.

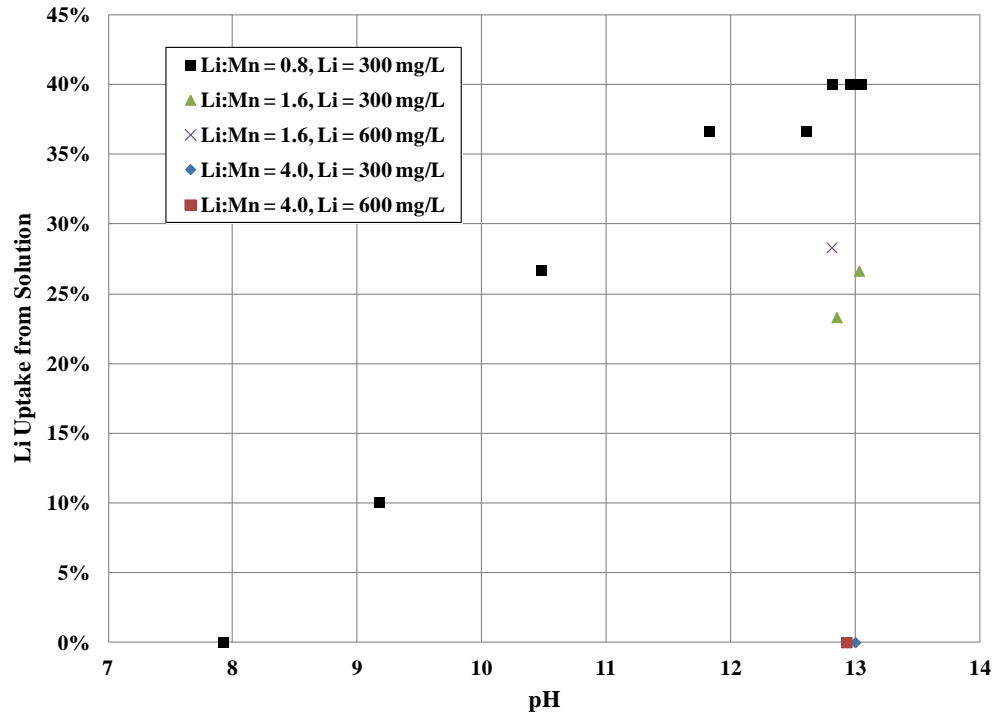


**Figure 7.2.** Li uptake on nano HMO. Li:Mn is on a mol:mol basis. Matrix is distilled water and the contact time = 1 hour.

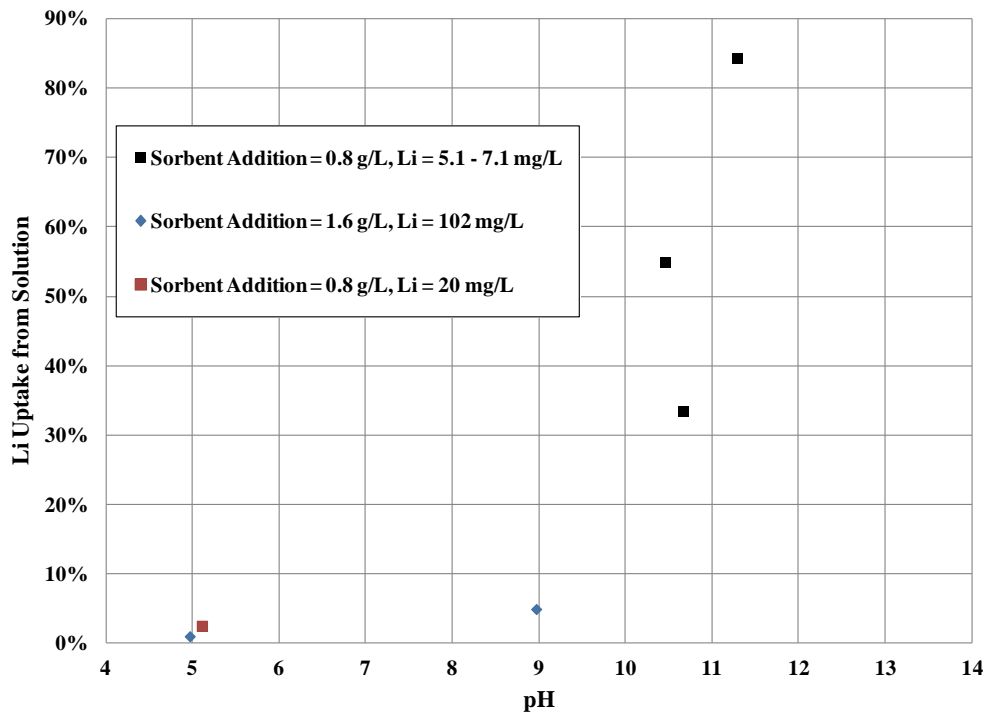


**Figure 7.3.** Li uptake on purchased LiMn<sub>2</sub>O<sub>4</sub>. Matrix is distilled water and the contact time is 24 hours.

The remaining solid sorbents were mixed together and subjected to the process of the sorbent preparation during which the solids were soaked in a 0.5 M HCl solution for 24 hours to extract the Li ions from the spinel-LiMn<sub>2</sub>O<sub>4</sub>. Following Li ion extraction, the sorbent was reacted with Li solution and the adsorption capability of the sorbent was recorded and analyzed.

Figure 7.4 shows the Li uptake on the hydrothermally produced LiMn<sub>2</sub>O<sub>4</sub>. Increasing the pH above 11.0, significantly increased the uptake of Li onto the sorbent. As mentioned above some uncertainty exists with the Li concentration measurements made by Carus utilizing the flame photometer especially at high pH. The Carus results are included in this section to show performance trends only, not absolute values. Table 7.1 shows the test conditions and full results from which Figure 7.4 were taken from.

The hydrothermally spinel-LiMn<sub>2</sub>O<sub>4</sub> was the most promising sorbent evaluated in the study. This sorbent shows promise for commercial development; however, additional testing, optimization, and confirmation of results on ICP-MS needs to be conducted. The sorbent must be evaluated under brine conditions also.

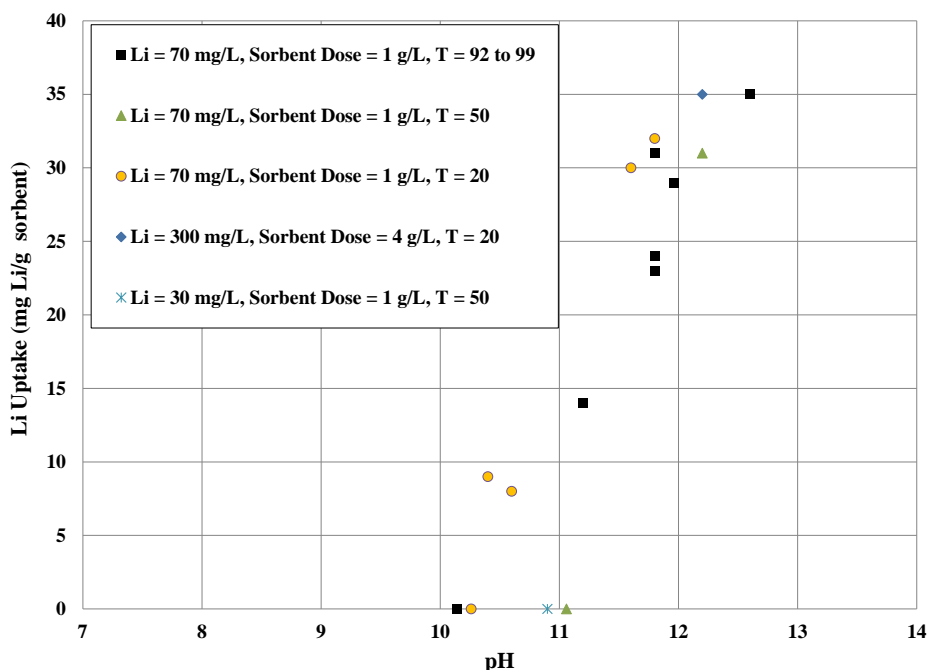


Figure 7.4. Li uptake on LiMn<sub>2</sub>O<sub>4</sub>. Matrix is distilled water and contact time is two hours.

**Table 7.1.** Li recovered from hydrothermally produced LiMn<sub>2</sub>O<sub>4</sub>.

Sample No.	Temp. (C°)	No. of Times Sorbent Reused	Matrix	Reactor Volume (mL)	pH	pH Adjustment Chemical	Sorbent Addition (g)	Li Source	Initial Li (mg/L)	Final Li (mg/L)	Li Sorption (mg Li/g sorbent)
1	20	4	Distilled Water	100	11.8	None	0.1	LiOH	70	38	32.0
2	20	5	Distilled Water	100	11.6	None	0.1	LiOH	70	40	30.0
3	50	4	Distilled Water	100	10.9	NaOH	0.1	LiCl	30	30	0.0
4	50	4	Distilled Water	100	11.1	NaOH	0.1	LiCl	70	70	0.0
5	96	5	Distilled Water	100	11.2	NaOH	0.1	LiCl	70	56	14.0
6	99	5	Distilled Water	100	11.8	NaOH	0.1	LiCl	70	46	24.0
7	50	5	Distilled Water	100	12.2	NaOH	0.1	LiCl	70	39	31.0
8	96	5	Distilled Water	100	12.6	NaOH	0.1	LiCl	70	35	35.0
9	20	4	Distilled Water	100	10.3	KOH	0.1	LiCl	70	70	0.0
10	20	5	Distilled Water	100	10.4	KOH	0.1	LiCl	70	61	9.0
11	94	5	Distilled Water	100	11.8	KOH	0.1	LiCl	70	47	23.0
12	99	5	Distilled Water	100	12.0	KOH	0.1	LiCl	70	41	29.0
13	94	5	Distilled Water	100	10.1	Ca(OH) <sub>2</sub>	0.1	LiCl	70	70	0.0
14	20	5	Distilled Water	100	10.6	Ca(OH) <sub>2</sub>	0.1	LiCl	70	62	8.0
15	92	5	Distilled Water	100	11.8	Ca(OH) <sub>2</sub>	0.1	LiCl	70	39	31.0
16	20	6	Distilled Water	100	12.2	NaOH	0.4	LiCl	300	160	35.0

***Li<sub>1.6</sub>Mn<sub>1.6</sub>O<sub>4</sub> (Southern Research)***

Southern Research produced Li<sub>1.6</sub>Mn<sub>1.6</sub>O<sub>4</sub> and conducted testing for recovery on simulated geothermal brines. The sorbent was produced by the method similar to that developed by Shi et al. with some changes [21].

Southern Research purchased LiMnO<sub>2</sub> and heated it in a furnace for 4 hours at 410 °C. The resulting sorbent was pickled in 0.5 N HCl for 2 hours. The pickled sorbent was washed with deionized (DI) water several times. The filtered sorbent was oven dried at 105 °C. The dried material was then collected and utilized for sorbent tests. The structure and form of the sorbent was not verified analytically.

The sorbent was evaluated for Li sorption to brines produced from the MD evaluations including 3 brines as described in Table 7.2. In addition to the brines shown in Table 7.2, the TDS of the high strength brine was also increased to approximately 250,000 mg/L by addition of NaCl.

**Table 7.2.** Brines utilized in the sorption experiments.

<b>Component</b>	<b>Low Strength (mg/L)</b>	<b>Medium Strength (mg/L)</b>	<b>High Strength (mg/L)</b>
<b>Ca<sup>2+</sup></b>	68	114	824
<b>Cl<sup>-</sup></b>	4,751	7,204	46,742
<b>Li<sup>+</sup></b>	40	64	456
<b>Mg<sup>2+</sup></b>	13	21	215
<b>Na<sup>+</sup></b>	2,995	4,345	30,192
<b>SO<sub>4</sub><sup>2-</sup></b>	5	18	138

For the low strength brine experiments, samples were prepared by mixing 1,000 mL with 1 g and 2 g of the sorbent. The pH of the bottle was raised to 12.0 using 20 ml of 0.2 N NaOH. After 1 hour contact time and agitation, samples of the solution were collected and filtered. Filtered samples were analyzed for Li. Similar samples were prepared for the medium strength brine except that 15 mL of 0.2 N NaOH solution was needed to raise the pH to 12.0.

For the high strength brine experiments, 50 mL of brine were contacted with 1 g of sorbent for 1 hour. The sorbent was then washed and the experiment was repeated. Experiments were

similarly conducted utilizing the 250,000 mg/L TDS brine except the pH could only be raised to 11.0 with the addition of 1.6 mL of 0.2 N NaOH solution. The sorbent was then washed and the experiment was repeated for the high strength brine and 250,000 mg/L brine.

Figure 7.6 shows that lower Li uptake was observed with this sorbent in the brine matrix compared to the other Mn-oxide sorbents in DI water. The maximum uptake for the high strength and 250,000 mg/L TDS brines varied from averages of 11.67 -12.06 mg Li/g sorbent. Secondary runs only increased the total uptake averages of 12.68 and 12.82 for the high strength and 250,000 mg/L brine, respectively.

The brine composition and method of sorbent preparation could have impacted the uptake of Li onto the sorbent. It may be that purchased  $\text{LiMnO}_2$  was not as crystalline as expected. It may be that production of the sorbent from raw materials may lead to a more effective sorbent.

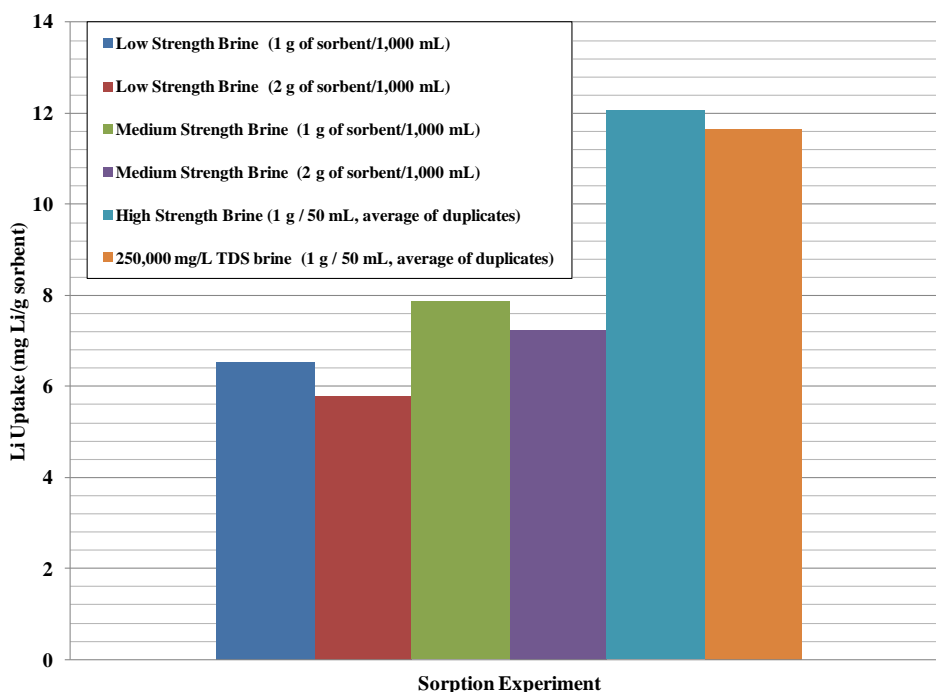


**Figure 7.6.** Li uptake from solution on  $\text{Li}_{1.6}\text{Mn}_{1.6}\text{O}_4$ . Contact time is 1 hour.

In addition, the pH was not measured at the end of the adsorption experiments. The pH may have dropped over the course of the experiment. Shi et al. achieved a maximum Li uptake of 27.15 mg/g and a Li adsorption rate of over 99% from a brine utilizing pH buffering in the process [21]. pH buffering could likely improve the process for the application described in this work.

The  $\text{Li}_{1.6}\text{Mn}_{1.6}\text{O}_4$  by utilized by Southern Research and verified by ICP-MS shows promise for further development under brine conditions. pH buffering to maintain high pH throughout the experiment could enhance the sorbent performance of the system. Future research and development for this process should focus on  $\text{Li}_{1.6}\text{Mn}_{1.6}\text{O}_4$ .

## 8.0 THERMOELECTRIC POWER GENERATION SYSTEM

The thermoelectric figure of merit  $Z\bar{T}$ , is a non-dimensional number consisting of three properties and the mean temperature across the material:

$$Z\bar{T} = \frac{\sigma S^2 \bar{T}}{k},$$

where  $\sigma$  is the electrical conductivity,  $S$  is the Seebeck coefficient, and  $k$  is the thermal conductivity. Each of these material properties are temperature dependent, which results in a temperature dependent  $ZT$ . However, two common approximations are to assume constant properties over a small temperature range or define effective properties that can be used over a large temperature range. The  $Z\bar{T}$  can be conveniently used to calculate the conversion efficiency which is the ratio of electric power to heat supplied on the hot side

$$\eta = \frac{W}{Q_{Hot}} = \frac{T_{Hot} - T_{Cold}}{T_{Hot}} \frac{\sqrt{1 + Z\bar{T}} - 1}{\sqrt{1 + Z\bar{T}} + \frac{T_{Cold}}{T_{Hot}}}.$$

There are many textbooks that describe thermoelectric principles, material characterization, testing and module design [23]. State of the art commercially available materials have  $ZT$  in the range of 0.8-1.2. Theoretically  $ZT$  can be as high as 15 for nanowires but have yet to be demonstrated. The highest credible report of high  $ZT$  is 2.4. The objective of this effort was to build and demonstrate basic operations of the integrated thermoelectric plus membrane distillation unit to validate the design of the commercial system. Ultimately this effort was successful.

### 8.1 *Thermoelectric Material Development*

Commercial  $\text{Bi}_2\text{Te}_3$ -base alloys are currently prepared by unidirectional crystal growth techniques such as Bridgeman and Czochralski. Unfortunately, materials processed by directional solidification suffer from poor mechanical strength and high thermal conductivity due to large grains and weak van der Waals bonding between Te (1) – Te (1) atoms, giving rise to easy cleavage along planes normal to the crystal's c-axis. The solid state synthesis approach used in this project overcomes these limitations by producing homogeneous materials from nanometric powders; and the high- $ZT$  enabling mechanisms such as nanostructuring and enhanced density of anti-site defects helped in our processing approach.

Mechanical alloying and hot pressing were used to achieve 25 mm diameter compacts. Rectangular bars were cut from the compacts for resistivity and Seebeck coefficient testing in an ULVAC ZEM-3.

## 8.2 *Thermoelectric Module Fabrication Results*

Modules built under this program were of the same module layout as commercial-off-the-shelf (COTS) modules to allow a direct comparison of the Novus hot pressed  $\text{Bi}_2\text{Te}_3$  with the COTS polycrystalline  $\text{Bi}_2\text{Te}_3$  module efficiency and performance. A 64 couple 4x4 cm module with hot pressed materials was fabricated and compared to a 64 couple 4x4 cm module made with COTS polycrystalline materials (Figure 8.1).

The 64 couple modules were tested by the independent contract laboratory (Custom Thermoelectric) that produced the modules. Testing results are provided in Figures 8.2 and 8.3. Testing has validated that Novus' nano-structured materials offer significantly lower thermal conductivity than COTS materials. This lower thermal conductivity results from the higher ZT of Novus materials. Lower thermal conductivity also translates to a larger  $\Delta T$  for Novus modules, for a given heat availability, and hence higher conversion efficiency. However, the overall performance of the module is on par with the COTS module.

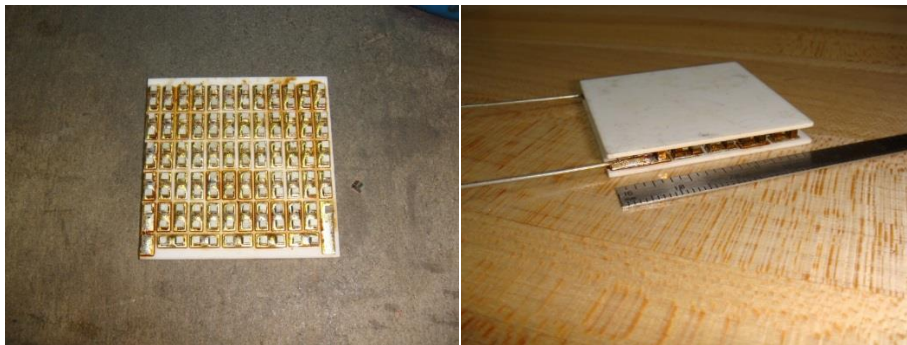


**Figure 8.1.** 64 couple module fabricated with Novus hot pressed p- and n-type  $\text{Bi}_2\text{Te}_3$  materials.

The reason for this is that the Novus TEG Module electrical contacts have not been fully optimized, and used standard contacts matching the COTS module. Even so, note that, in spite of less heat draw at each  $\Delta T$ , the Novus module offers as good an efficiency as COTS, in spite of non-optimal electrical contacts. When Novus TEG Modules are fully optimized for electrical contacts, it is expected that a significant improvement in heat-to-electric conversion efficiency will be observed. Modeled results for efficiency based on optimized contacts are provided in

Figure 8.4. It is anticipated that a 6% conversion efficiency for  $\Delta T \sim 125^\circ\text{C}$  will be achieved based on current results and module optimization.

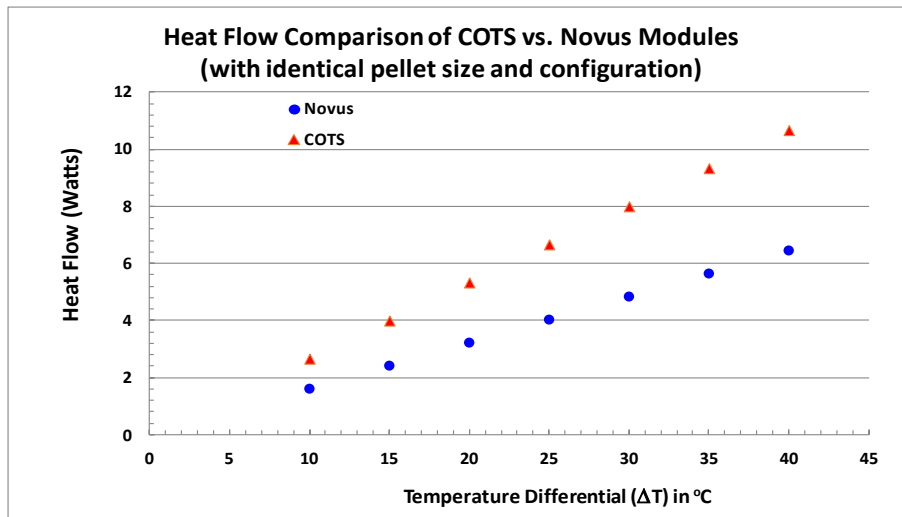


Figure 8.2. Heat flow comparison for COTS versus Novus modules, non-optimized contacts.

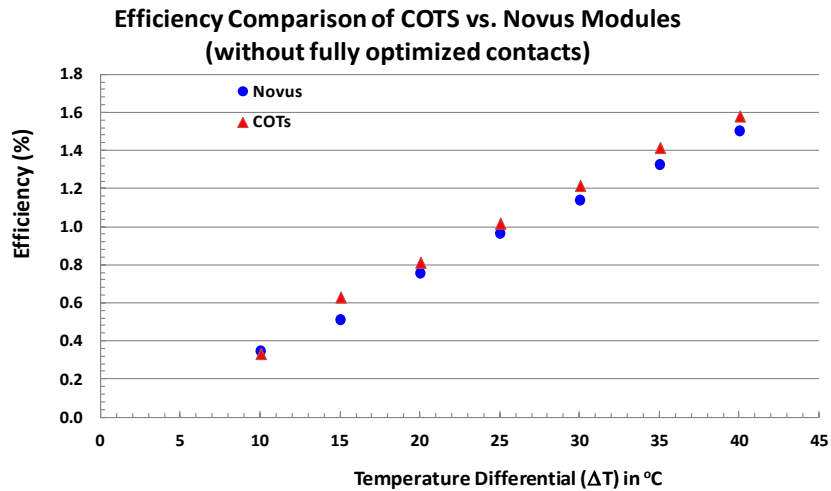
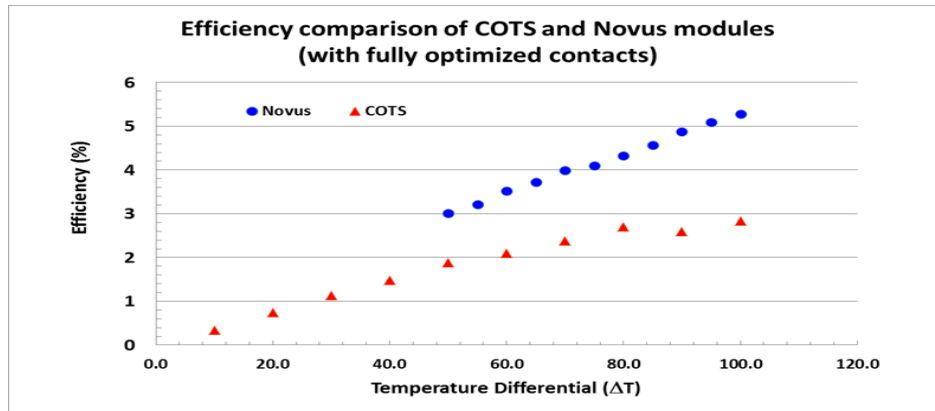


Figure 8.3. Efficiency comparison for COTS versus Novus modules, non-optimized contacts.



**Figure 8.4.** Efficiency comparison of COTS and Novus modules with fully optimized contacts.

### 8.3 *Integrated Membrane Distillation – Thermoelectric Generator Module Development*

The integrated MD-TEG test module was designed, built, and used to evaluate the viability of utilizing the TEG unit and temperature differential driven by the cold side heat exchanger to both generate electric power and to drive the temperature driven membrane distillation process. The integrated module was designed to allow for flexibility in utilization of different 4cm x 4cm TEG modules, as well as different membranes. The module also includes a viewing port to allow observation of flow in the module chamber for visual evaluation of things like stagnation, steam generation, and membrane fouling/rupture. There are several design configurations for traditional MD systems such as system with an air gap or vacuum air gap between the membrane and condenser. In this design we used a wick where the air gap might have been, it provides mechanical support to the membrane, and simplifies the design and characterization of the system. The area of the thermoelectric to membrane is matched 1:1 which again simplifies the construction and characterization of the system. Heat loss was another design concern. In response to this, the hot side is constructed of low thermal conductivity materials (Teflon, glass) and the heat exchanger (water block) on cold side is sized just big enough for the TE module. Integrated module designs are provided in Figure 8.5. Actual photographs of the assembled unit are provided in Figure 8.6.

The test rig design is provided in Figure 8.7 showing energy and mass flows in the system. The membrane was supplied by AMT (Applied Membrane Technologies). It had a base material composed of a hydrophobic PTFE membrane filter with a 5.0 micron pore size and then coated with a custom tailored superhydrophobic Parylene coating on both sides. The AMT coating reduced the original pore size below 5 microns and also added strength to the base material. Both

the base PTFE material and the AMT layers of superhydrophobic Parylene can tolerate temperatures of 260 °C or higher.

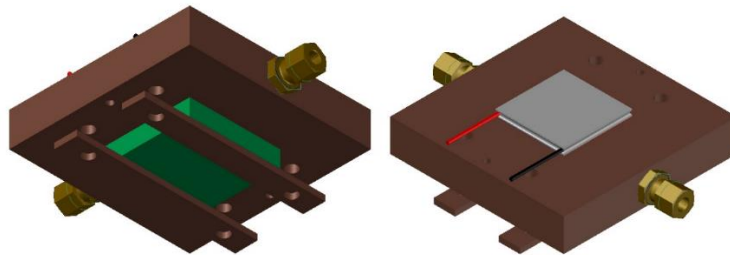


**Figure 8.5.** Integrated MD-TEG test module design showing glass viewport (L) and TEG module (without water block heat exchanger) (R).

The TEG MD prototype was tested under fluid stream conditions of 50-95°C (smaller than the commercial temperature range of 150°C on the hot side) on the hot side and 25°C on the cold side to avoid requirements for elevated pressures due to presence of significant water vapor. Temperatures are measured at the cold/hot fluid inlet/outlet, using four thermocouples in all. The first experimental set-up tested the prototype without a membrane installed, then a second set-up was evaluated with a membrane installed, allowing for comparison of the thermal performance with and without the membrane and calculation of the thermal properties of the membrane. The thermoelectric module (TEM) was a COTS product with known properties provided on a specifications sheet which were used in the analysis to infer what the actual temperature drop was across the TEM in lieu of thermocouples in those positions.

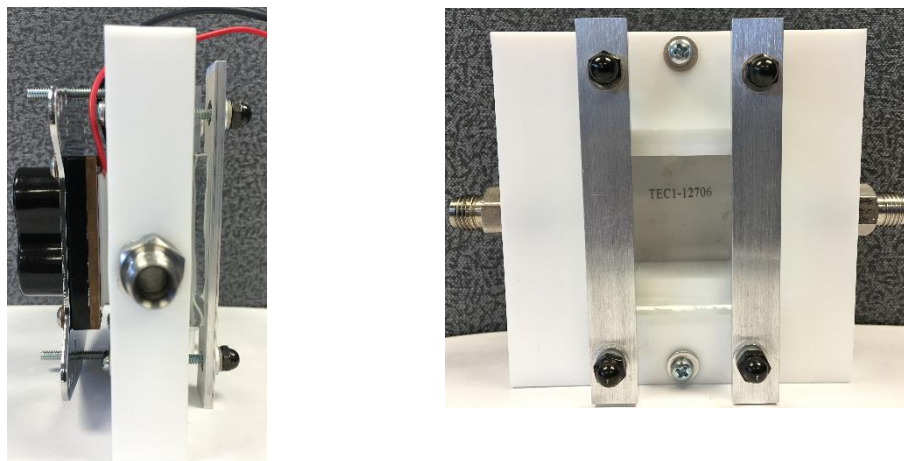
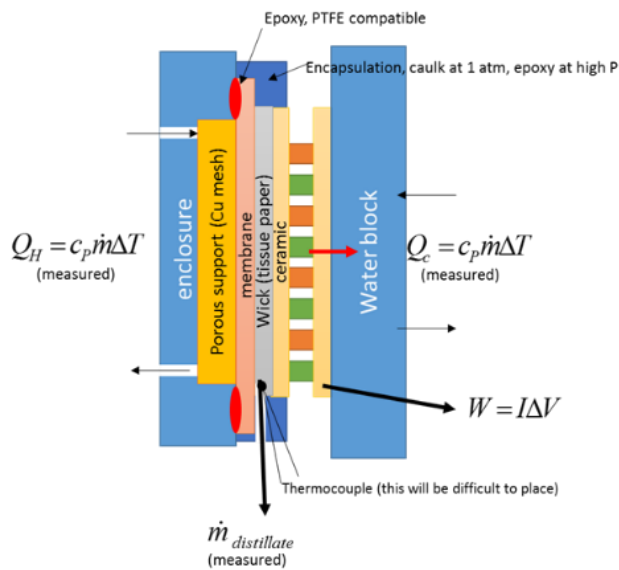


**Figure 8.6.** MD-TEG test module showing (L) stacked module with water block (cold side heat exchanger), TEG module, brine chamber, glass viewing block and (R) view through glass block of chamber and TEG module.

## Experimental design



### Instrumentation

$Q_H$ : 2 TCs  
 $Q_C$ : 2 TCs  
 $TH\_module$ : 1 TC  
 $TC\_module$ : 1 TC  
 $T\_distillate$ : 1 TC

VTE: portable multimeter  
 I: portable multimeter or DAQ

**Figure 8.7.** Experimental Test Rig design, identifying heat and mass flows to be monitored and instrumentation used for data collection.

Results are provided in Figure 8.8. Note that  $Q_{hot}$  and  $Q_{cold}$  are measured for each of the fluid streams, and the values are approximately equal which indicates the thermal losses in the system are minor. The triangles are calculated from the manufactures' thermoelectric property data and using the measured open circuit voltage to infer the temperature difference across the module. The agreement is good between the calculated and measured values.

Figure 8.9 shows open circuit voltage versus average temperature of hot side fluid stream. The measured voltage is less than the calculated ideal values due to thermal resistance on either side of the TEM reducing the temperature drop across the module. Heat transfer is further impeded with the membrane in place especially at low temperatures, but the difference becomes smaller as the temperature (and vapor pressure) of the hot side increases. Wick one was chromatography paper with thickness of 0.290 mm and wick two was cheesecloth at a thickness of 0.135. There is no apparent difference in performance difference between the two wicks.

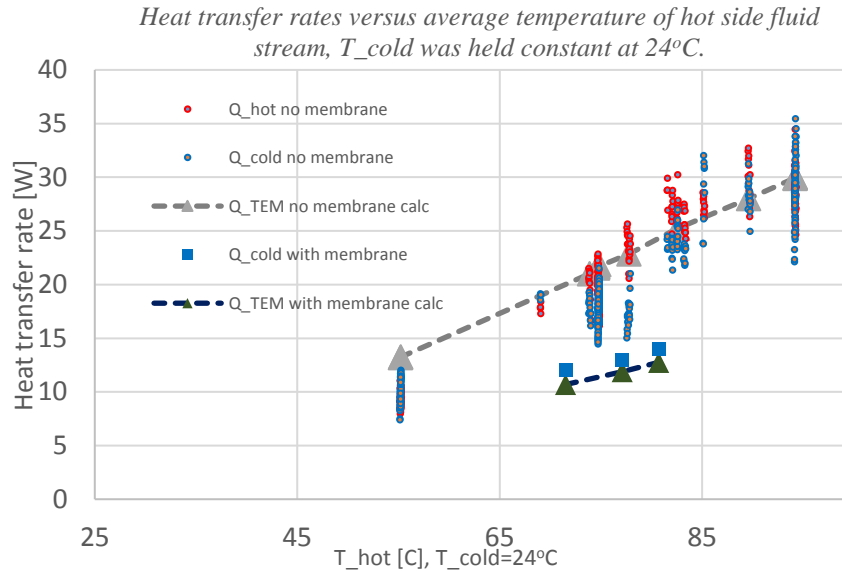


**Figure 8.8.** Heat transfer rates versus average temperature of hot side fluid stream,  $T_{cold}$  was held constant at 24 °C. Experimental points show significant scatter but are consistency with the modeled result.

The system reached state steady quickly (5 min), which was much faster than the time it took the hot water bath to reach a new set point. The design was successful in minimizing heat loss. The hot side and cold side heat transfers agree well for  $T_{hot} < 75^{\circ}\text{C}$ , and  $Q_{hot}$  becomes larger than  $Q_{cold}$  for  $T_{hot} > 75^{\circ}\text{C}$ , which is expected due to heat loss at the polymer block and hot side window. The hot side window was useful for troubleshooting the system such as to ensure air was not trapped inside the chamber. The characterization of the TEM properties given by the manufacturer was consistent with our measurements of heat flow. This allows us to confidently infer what the actual temperature drop over the TEM is by using the open circuit voltage and allows us to back-out thermal properties of the membrane. Primary findings were that the concept is successful in both producing a distillate product as well as producing electric power. Due to the very small scale of the module system and the reduced operating temperature of the hot side, the amount of power and the amount of distillate produced were small. Produced power was on the order of 0.12 W at a  $\Delta T$  of 68 °C on the inlets, equivalent to an estimated 31 °C  $\Delta T$  across the TEM. Distillate was not collected from the wick paper – it either evaporated or produced only several drops of liquid.

*Open circuit voltage versus average temperature of hot side fluid stream,  $T_{cold}$  was held constant at 24°C.*

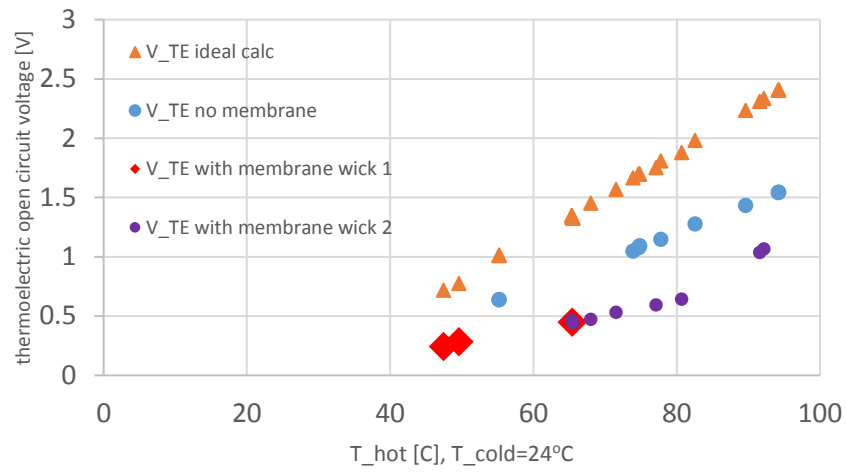


**Figure 8.9.** Open circuit voltage versus average temperature of hot side fluid stream,  $T_{cold}$  was held constant at 24 °C.

## 9.0 TECHNICAL AND ECONOMIC ANALYSIS

First, a techno-economic analysis of the TEG/membrane distillation/lithium recovery system was developed using the DOE’s generic proforma tool (Revision 1). A model was developed for a recovery plant, co-located at a geothermal power generating station, capable of treating 500 gpm of brine flow with Li content of 150 mg/L. The TEG efficiency assumed was 5.24%. The process equipment was sized using cost information from various sources and general scaling laws. A simple economic analysis was conducted to determine the minimum selling price for a lithium carbonate ( $\text{Li}_2\text{CO}_3$ ) product stream while maintaining a 10% internal rate of return (IRR).

In order to generate the capital cost, all the major equipment costs were estimated for an Nth plant of 500 gpm with incoming brine temperature of 150°C. The analysis assumed a high strength brine concentration which can be found in Table 9.1.

**Table 9.1.** Incoming brine composition for techno economic analysis

Component	Conc. (mg/L)
$\text{Ca}^{2+}$	417.7
$\text{Mg}^{2+}$	240.9
$\text{Na}^+$	7,339.6
$\text{Cl}^-$	12,918.8
$\text{SO}_4^{2-}$	440.4
$\text{Si}^{4+}$	87.5
$\text{Li}^+$	150
$\text{K}^+$	621.3

The major equipment considered for the analysis consisted of silica removal/filtration, the nano-filtration system, the thermo-electric generator (TEG), two membrane distillation stages, the lithium recovery adsorbers, and the required cooling tower and heat exchangers.

The concept for the silica removal was revised some from the original concept. The concept now includes raising the pH to approximately 9.0 followed by ultrafiltration with ceramic membranes at the high temperatures encountered. The concept no longer includes a large settling tank for silica removal. Figure 9.1 shows the revised concept (compare with Figure 3.1). The ultrafiltration costs were acquired from a vendor as the system is an off the shelf system. Disposal of the ultrafiltration reject was not considered in the estimate.

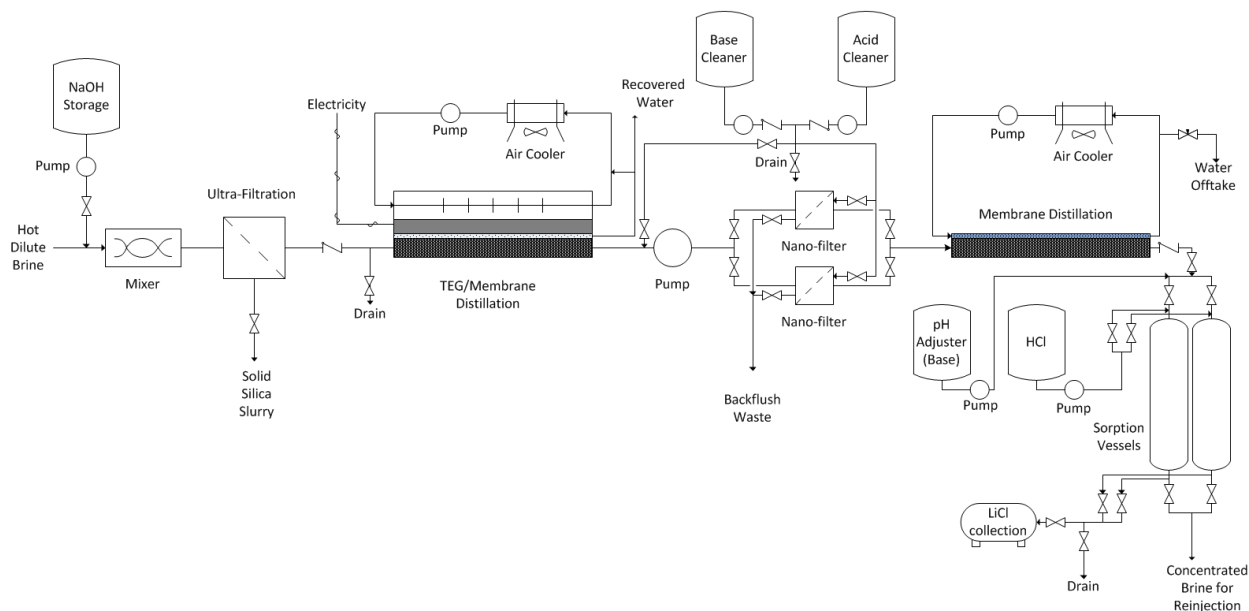


**Figure 9.1.** Revised concept showing pH adjustment plus ultrafiltration to remove silica.

The nano-filtration costs were estimated using costs for reverse osmosis systems for desalination [24]. It was assumed that the nano-filtration system would cost approximately half the amount of the desalination equipment capital costs produced by Dow for similar flow rates. The costs for the TEG were assumed to be the end targets of the project: \$0.40/watt, while the electrical output was calculated at 5.24% efficiency due to flux matching with the ceramic membrane distillation. The membrane distillation system price was given as \$/m<sup>2</sup> of membrane area, provided by equipment supplier and project partner AMT. The Li recovery adsorbers consisted of three columns filled with manganese sorbent (sorbent costs included). Two of the columns would switch back and forth hourly to collect lithium from the brine. The third column would be in regeneration mode. Upon completion of the regeneration cycle, it would switch with one of the active columns. The columns were sized to operate a few days between regeneration cycles, and the equipment cost was estimated as if they were packed horizontal vessels using the NETL Process Equipment Cost Estimation (PECE) report [25]. Finally, the costs for the cooling towers – required to maintain the  $\Delta T$  across the membrane distillation and TEG loops – were also estimated using the NETL PECE report. The total overall installed cost for each subsystem can be found in Table 9.2. The Total Capital Cost was determined as the installed costs multiplied by a Lang factor of 3.5.

**Table 9.2.** Subsystem costs for pro-forma

	Cost
Silica Removal/Ultrafiltration Cost	\$ 600,000
TEG/membrane Cost	\$ 739,680
Nano-filtration Cost	\$ 581,625
Membrane Distillation Cost	\$ 1,970,015
Li Recovery Cost	\$ 1,703,358
Pumping Costs	\$ 46,000
Cooling Towers/ Heat Exchanger Cost	\$ 719,758
Total Installed Cost	\$ 6,360,436
Total Capital Cost	\$ 22,261,526

The capital costs were input into the DOE’s generic proforma tool, along with Li production rates, electricity generation/consumption, and chemical usage to develop the pro-forma. All additional heat required for the membrane distillation would be provided using supplemental heat from available excess brine. The values used for expense rates are presented in Table 9.3.

**Table 9.3.** Assumed expense rates

Inflation Rate	Fixed at 2.4%	
Interest Rate on Debt	Fixed at 8%	
Term of Loan	15 years	
Payroll & Benefits	% of Revenue	20.0%
Fixed Operating Expenses	% of Revenue	1.0%
Annual Maintenance	% of Capex	2.5%
Corporate Overhead	% of Revenue	8.0%
Insurance	% of Capex	2.0%
Property Tax	% of Capex	4.0%
Management Fees	% of Revenue	4.0%
Contingency	% of O&M, G&A	5.0%

For the fixed costs a simple assumption that the cost of electricity would be the same whether it was excess generated or electricity consumed by the process. Table 9.4 shows the unit cost of other fixed expenses.

Using these inputs several variables were adjusted to find the minimum selling price of the lithium product to maintain a 10% IRR (see Figure 9.2).

Analysis was also conducted using a discounted cash flow (DCF) analysis and net present value (NPV) calculation. All data from the proforma were therefore incorporated into a discounted cash flow analysis, which consisted of a three-year construction period (where equal portions of the overall plant capital cost is paid) followed by a 15-year operating period, utilizing an 18.5% depreciation rate and a 2.4% growth rate.

**Table 9.4.** Assumed fixed expense rates

Fixed Cost Items	Rates	
Sodium Hydroxide	\$/metric ton	400
HCl	\$/metric ton	85.28
Mn Sorbent	\$/metric ton	10,000
Net Electricity Consumed	\$/kWh	0.05453

The selling price of lithium carbonate is volatile and subject to short-term and local aberrations. In the past year, the price in China has more than tripled [26]. The base case price for the NPV/DCF analysis was \$20,000 per ton.

According to Teheri, a typical discounted cash flow analysis does not properly account for the risk associated with mining projects [27]. Instead it is suggested that a risk adjusted discount rate should be used in discounted cash flow evaluations. Table 9.5 shows the associated premiums for different types of projects depending on the stage of development or the aim of the project. For the purposes of this analysis, the project has been designated an early exploration project that is a new construction project. This combination is inherently the most risky type of project which can be seen in the ranges presented in the matrix shown in Table 9.6.

Based on the initial techno-economic analysis using the pro-forma, it was found that as with many new technologies, the current design of the process does not fare well in the analysis. Plants size did not prove to be a major driving factor as none of the studied sizes with an initial Li concentration of 150 mg/L could overcome the startup barrier imposed by the initial capital cost to be competitive in the current market. However, plants that had much higher Li concentrations quickly saw their minimum selling price drop quite substantially. Plants with a higher Li concentration were more profitable primarily because they could capture more lithium while utilizing the same sized equipment. The profitability of these plants, however, would be highly dependent on the price of Li. A 500 GPM plant with Li concentrations of 300 mg/L would produce

about 650-780 metric ton/yr of  $\text{Li}_2\text{CO}_3$ , which is a considerable portion of the total world Li market, and it would be a significant production for the American market.

**Table 9.5.** Premiums associated with project stage and project category.

	Risk Premium		Premium/Discount
Operating Mine	0%	Aimed at improving an existing Project	-(3-5%)
Feasibility Study	3-5%	Used to expand production	0%
Pre-feasibility Study	6-8%	Adding a new project to an existing complex	8-10%
Early Exploration	10-12%		

**Table 9.6.** Risk premium project matrix.

	Operating Mine	Feasibility Study	Pre-feasibility Study	Early Exploration
Aimed at improving an existing Project	-(3-5)%	0	3%	7%
Used to expand production	0%	3-5%	6-8%	10-12%
Adding a new project to an existing complex	8-10%	11-15%	14-18%	18-22%

The base case for the discounted cash flow evaluation shows that the investment would not net an attractive return unless the price of lithium carbonate would be about \$28,000/metric ton as shown in Figure 9.3. However, if capital costs could be reduced by ~27% then a breakeven point could be reached with Li prices of \$20,000 /metric ton as shown in Figure 9.4.

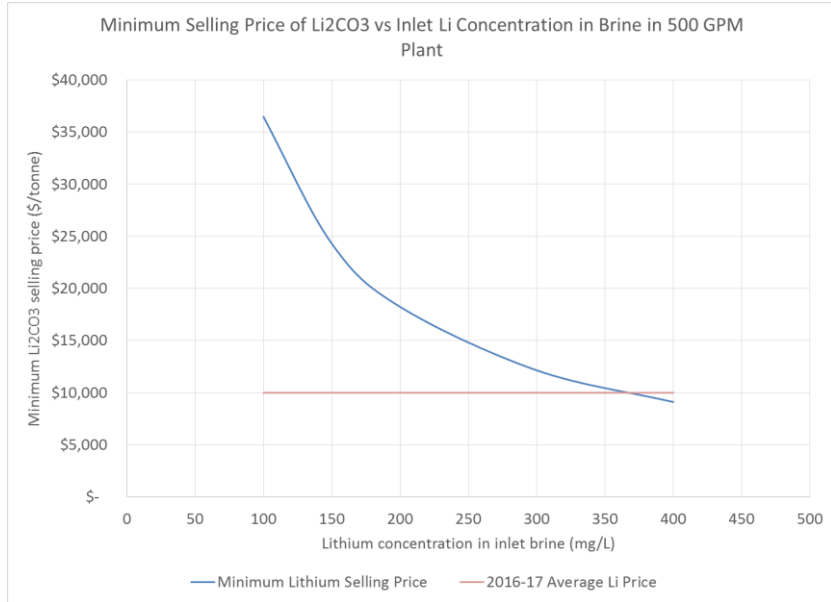


**Figure 9.2.** Minimum Li selling price versus plant size; and minimum Li selling price for 500 GPM Plant as a function of brine concentration.

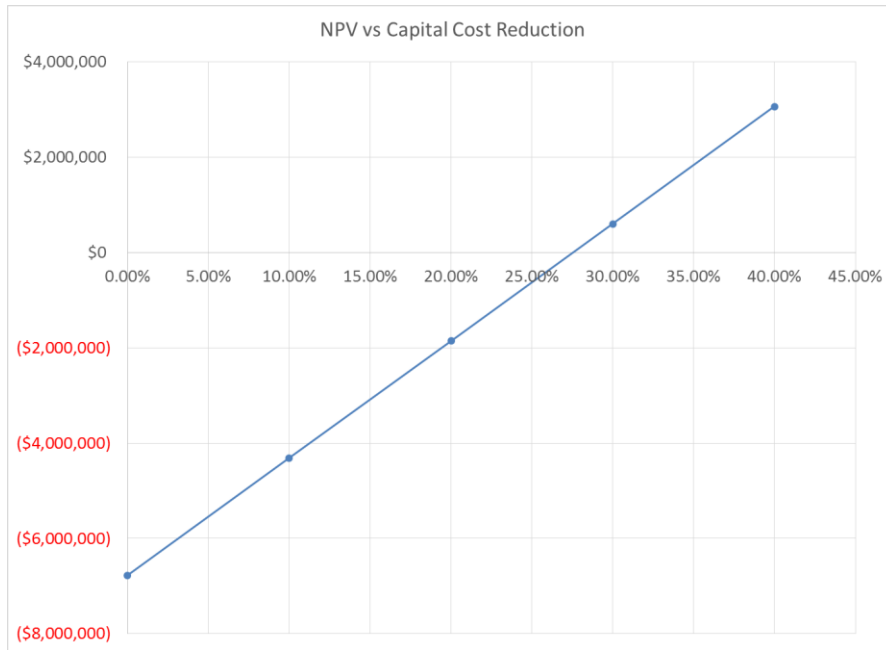


**Figure 9.3.** Net present value versus amount of capital cost reduction for a 500 GPM plant with 150mg/L Li concentration.

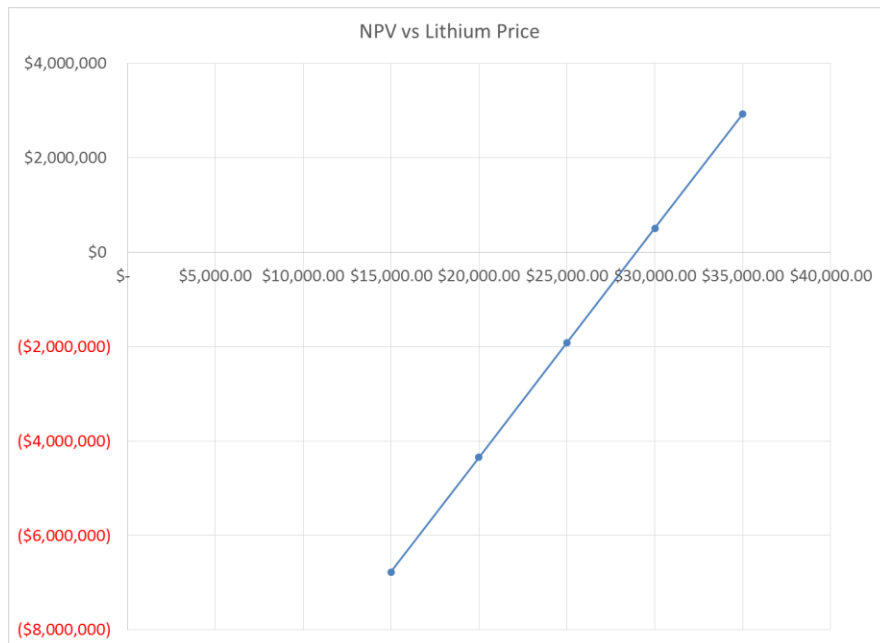


**Figure 9.4.** Net present value vs  $\text{Li}_2\text{CO}_3$  selling price for a 500 GPM plant with 150 mg/L Li concentration

From the analysis presented above, the economics appear unfavorable for an integrated lithium recovery process installation based on the proposed technology in its current state. In the absence of higher brine Li concentrations or lithium product selling prices, there remain several opportunities for design improvement and optimization that would allow for commercial deployment. The areas with the greatest potential impact on improving the economics involve membrane distillation performance and the lithium adsorber equipment design.

With the current design, the surface area of the first membrane distillation stage is sized according to the specified surface area for the TEG module. However the flux capability of the current membrane technology (constructed of high temperature tolerant materials) does not achieve the requirements for the TEG system, and this mismatch results in the TEG operating at reduced efficiency. With improvements to the membrane flux performance, the added electric generation from the TEG, operating at higher efficiency, would provide additional revenue for the recovery plant. Further, an optimized TEG-membrane system design is expected to reduce the overall component costs from the current value of \$5,250/m<sup>2</sup>. Improvements to the second membrane distillation stage would also have a significant impact on the overall system economics. Currently, the second-stage MD system represents 31% of the total installed costs, primarily due to its large surface area requirement (>2,600 m<sup>2</sup>). Improvements to the flux performance of this stage would reduce the surface area requirements and, consequently, installed equipment costs.

Finally, the Li adsorbers were sized based on limited data from evaluations on non-optimized sorbents. To more accurately specify the equipment sizing and sorbent usage requirements, experiments are necessary to develop adsorption isotherm and breakthrough characteristics for the actual sorbent and feed brine stream. Also, further work is needed to improve/optimize the Li adsorptive capacity for the selected sorbent. These efforts could result in reducing the column size and sorbent usage, as well as increasing the column operating period between regeneration cycles, which subsequently, reduces both installation and operating costs.

## 10.0 CONCLUSIONS

The overall project has proven to be successful by achieving several of the target milestones. It was demonstrated under several scenarios that the silica removal goal (>80%) could be achieved by increasing the brine pH and adding  $\text{Fe}^{3+}$ . The NF process was able to achieve approximately 80%  $\text{Ca}^{2+}$  and  $\text{Mg}^{2+}$  removal while rejecting <25% Li for high strength brines. MD experiments demonstrated that geothermal brines could be significantly concentrated with little fouling due to the pre-treatment processes (i.e. upstream silica removal and NF softening). Although the experiments using the Mn-oxide sorbent did not achieve the lithium uptake goal of 50 mg Li/g sorbent, actual results were promising with lithium uptake performance at ~12 mg/g using non-optimized sorbent material ( $\text{Li}_{1.6}\text{Mn}_{1.6}\text{O}_4$ ) in simulated brine. With optimization and further testing under actual brine conditions, it is expected that the Li adsorptive capacity could be improved, and the selected Mn-oxide sorbent will achieve performance closer to that of the project goal. The thermo-electric module showed a higher ZT which reduces the heat loss across the thermo-electric while increasing electrical generation efficiency. However, additional development and optimization in auxiliary components such as contactors are needed to show significant gains over current technologies. The integrated TEG system with distillate wick demonstrated that the preliminary design of the system could generate both electricity and distillate.

The economics for the installation of a fully integrated recovery process as designed were determined to be unfavorable unless the right local conditions exist – the most critical being Li concentration (well with greater than 300 mg/L Li concentrations) and Li selling price (>\$20,000/ton). For more modest brine lithium concentrations (~150 mg/L) and product selling prices (\$10,000 – \$15,000/ton), additional process improvements are necessary – higher MD flux performance, increased sorbent capacity, e. g. Though the proposed technology is in the early stages of development, the results from this study indicate that further investigation is warranted. The technology would stand to benefit greatly from targeted optimization on process subsystems.

Future development work must include determining the adsorption isotherm and column performance characteristics for the Mn-oxide sorbent in actual brine conditions. This is necessary to accurately design a full-scale system. In addition, pilot scale testing of the fully integrated process should be conducted after optimizing the individual components for maximized efficiency.

## 11.0 REFERENCES

1. Cheng, H.-H., S.-S. Chen, and S.-R. Yang, *In-Line Coagulation/Ultrafiltration for Silica Removal from Brackish Water as RO Membrane Pretreatment*. Separation and Purification Technology, 2009. **70**(1): p. 112-117.
2. Thomas, D.M., *Silica Recovery and Control in Hawaiian Geothermal Fluids*. 1992.
3. Murthy, Z.V.P. and A. Choudhary, *Application of Nanofiltration to Treat Rare Earth Element (Neodymium) Containing Water*. Journal of Rare Earths, 2011. **29**(10): p. 974-978.
4. *An Integrated Framework for Treatment and Management of Produced Water - Technical Assessment of Water Treatment Technologies*. 2009, Colorado School of Mines.
5. Murthy, Z.V.P. and L.B. Chaudhari, *Application of Nanofiltration for the Rejection of Nickel Ions from Aqueous Solutions and Estimation of Membrane Transport Parameters*. Journal of Hazardous Materials, 2008. **160**(1): p. 70-77.
6. Murthy, Z.V.P. and A. Choudhary, *Separation of Cerium from Feed Solution by Nanofiltration*. Desalination, 2011. **279**(1-3): p. 428-432.
7. Kharaka, Y.K., et al., *Removal of Selenium from Contaminated Agricultural Drainage Water by Nanofiltration Membranes*. Applied Geochemistry, 1996. **11**(6): p. 797-802.
8. Somrani, A.A.H.H.a., M. Pontie, *Study on Lithium Separation from Salt Lake Brines by Nanofiltration (NF) and Low Pressure Reverse Osmosis (LPRO)*. Desalination, 2013. **317**: p. 184-192.
9. Wen, X., P. Maa, C. Zhua, Q. Hea, and X. Denga, *Preliminary Study on Recovering Lithium Chloride from Lithium-Containing Waters by Nanofiltration*. Separation and Purification Technology, 2006. **49**: p. 230-236.
10. Gang, Y., S. Hong, L. Wenqiang, X. Weihong, and X. Nanping, *Investigation of  $Mg^{2+}/Li^{+}$  Separation by Nanofiltration*. Chinese Journal of Chemical Engineering, 2011. **19**(4): p. 586.
11. *Molecular weight cut-off*. 2017 [cited 2017].
12. Alkhubhri, A., N. Darwish, and N. Hilal, *Membrane Distillation: A Comprehensive Review*. Desalination, 2012. **287**(0): p. 2-18.
13. Martinez-Diez, L., and F.J. Florido-Diaz, *Desalination of Brines by Membrane Distillation*. Desalination, 2001. **137**: p. 267-273.
14. Gryta, M., *The Concentration of Geothermal Brines with Iodine Content by Membrane Distillation*. Desalination, 2013. **325**: p. 16-24.
15. Camacho L.M., L.D., J. Zhang, J. Li, M. Duke, J. Gomez, and S. Gray *Advances in Membrane Distillation for Water Desalination and Purification Applications*. Water, 2013. **5**: p. 94-196.
16. Sirkar, K.K., and L. Song, *Pilot-Scale Studies for Direct Contact Membrane Distillation-Based Desalination Process*. 2009, U.S. Department of the Interior Bureau of Reclamation: U.S. Department of the Interior Bureau of Reclamation.
17. El-Bourawi, M.S., Z. Ding, R. Maa, and M. Khayet, *A Framework for Better Understanding Membrane Distillation Separation Process*. Journal of Membrane Science, 2006. **285**: p. 4-29.
18. Gryta, M., *Concentration of NaCl Solution by Membrane Distillation Integrated with Crystallization*. Separation Science and Technology, 2002. **37**(15): p. 3535-3558.

19. Chitrakar, R., H. Kanoh, Y. Miyai, and K. Ooi, *Recovery of Lithium from Seawater Using Manganese Oxide Adsorbent ( $H_{1.6}Mn_{1.6}O_4$ ) Derived from  $Li_{1.6}Mn_{1.6}O_4$* . Industrial & Engineering Chemical Research, 2001. **40**: p. 2054-2058.
20. Kitajou, A., T. Suzuki, S. Nishihama, and K. Yoshizuka, *Selective Recovery of Lithium from Seawater using a Novel  $MnO_2$  Type Adsorbent II - Enhancement of Lithium Ion Selectivity of the Adsorbent*. Ars Separatoria Acta, 2003. **2**: p. 97-106.
21. Shi, X., D. Zhou, Z. Zhang, L. Yu, H. Xu, B. Chen, and X. Yang, *Synthesis and Properties of  $Li_{1.6}Mn_{1.6}O_4$  and its Adsorption Application*. Hydrometallurgy, 2011. **110**: p. 99-106.
22. Liddle, B.J., S.M. Collins, and B.M. Bartlett, *A New One-Pot Hydrothermal Synthesis and Electrochemical Characterization of  $Li_{1+x}Mn_{2y}O_4$  Spinel Structured Compounds*. Energy & Environmental Science, 2010. **3**: p. 1339–1346.
23. Rowe, D.M., *Thermoelectrics Handbook Macro to Nano*. 2006: CRC Taylor & Francis.
24. Beardsley, S., S.D. Coker, and S.S. Whipple, *The Economics of Reverse Osmosis and Ion Exchange*, in *Watertech*. 1994: Houston, Texas.
25. Loh, H.P., J. Lyons, and C.W. White, *Process Equipment Cost Estimation*. 2002, U.S. Department of Energy: National Energy Technology Laboratory.
26. *What Price Lithium, the Metal of the Future?* 2016 [cited 2017; Available from: <http://fortune.com/2016/06/06/lithium-price-tesla-metal-future/>].
27. Epstein, P. *Getting to Grips with the Lithium Market*. 2016 [cited 2016; Available from: <http://www.mineweb.com/news/industrial-metals-and-minerals/getting-to-grips-with-the-lithium-market/>].